REPORT DOCUMENTATION PAGE

Form Approved
OMB No. 0704-0188

1. REPORT DATE	2. REPORT TYPE	3. DATES COVERED *(From - To)*
21 May 2018	Conference Paper with Briefing Charts	01 May 2018 - 06 February 2019

4. TITLE AND SUBTITLE
Preliminary Study of the Reacting Flow from Multi-Element Shear Coaxial Flows (Conference Paper with Briefing Charts)

5a. CONTRACT NUMBER

5b. GRANT NUMBER

5c. PROGRAM ELEMENT NUMBER

6. AUTHOR(S)
M. Roa and D. Talley

5d. PROJECT NUMBER

5e. TASK NUMBER

5f. WORK UNIT NUMBER
Q0YA (49221249)

7. PERFORMING ORGANIZATION NAME(S) AND ADDRESS(ES)
Air Force Research Laboratory (AFMC)
AFRL/RQRC
10 E. Saturn Blvd.
Edwards AFB, CA 93524-7680

8. PERFORMING ORGANIZATION REPORT NUMBER

9. SPONSORING/MONITORING AGENCY NAME(S) AND ADDRESS(ES)
Air Force Research Laboratory (AFMC)
AFRL/RQR
5 Pollux Drive
Edwards AFB, CA 93524-7048

10. SPONSOR/MONITOR'S ACRONYM(S)

11. SPONSOR/MONITOR'S REPORT NUMBER(S)
AFRL-RQ-ED-TP-2019-048

12. DISTRIBUTION/AVAILABILITY STATEMENT
Distribution Statement A: Approved for Public Release; Distribution is Unlimited. PA Clearance Number: 19071 Clearance Date: 06 February 2019.

13. SUPPLEMENTARY NOTES
For presentation at JANNAF; Long Beach, CA, USA; May 21, 2018 (Presented at May 2018 JANNAF as Distribution C package - now being re-released with no changes - as a Distribution A package). Prepared in collaboration with Sierra Lobo, Inc.
The U.S. Government is joint author of the work and has the right to use, modify, reproduce, release, perform, display, or disclose the work.
Conference Paper with Briefing Charts.

14. ABSTRACT
The reacting flow dynamics from a linear array of three shear coaxial injectors operating under sub-critical pressures was investigated. High-speed images recorded the center injector's response and behavior under the influence of its neighboring injectors for both acoustically unforced and forced conditions. The injectors employed liquid rocket engine relevant propellants of gaseous hydrogen and liquid oxygen. High-speed shadowgraph images along with OH* chemiluminescence captured the hydrodynamic instabilities for each injector and the flame interactions. Overlapping OH* chemiluminescence on top of the shadowgraph images, similar vortex/flame interactions were observed as were observed for a single jet for each individual jet from the injector. Spectral analysis on the OH* chemiluminescence in the near field shows that the individual flames share similar frequency fluctuations when the multi-element array was not subjected to acoustic forcing. These frequencies were also present in the dynamic mode decomposition of the shadowgraph and OH* chemiluminescence images used to investigate the modal structures of both the LOX jet and flame, respectively. Under acoustic forcing, the modal structures of both the LOX jet and flame are the same from each injector.

15. SUBJECT TERMS
N/A

16. SECURITY CLASSIFICATION OF:			17. LIMITATION OF ABSTRACT	18. NUMBER OF PAGES	19a. NAME OF RESPONSIBLE PERSON
a. REPORT	b. ABSTRACT	c. THIS PAGE			D. Talley
Unclassified	Unclassified	Unclassified	SAR	35	19b. TELEPHONE NUMBER *(Include area code)* N/A

PRELIMINARY STUDY OF THE REACTING FLOW FROM MULTI-ELEMENT SHEAR COAXIAL FLOWS

Mario Roa
Sierra Lobo, Inc.
Edwards AFB, CA

Douglas. G. Talley
Air Force Research Laboratory
Edwards AFB, CA

ABSTRACT

The reacting flow dynamics from a linear array of three shear coaxial injectors operating under sub-critical pressures was investigated. High-speed images recorded the center injector's response and behavior under the influence of its neighboring injectors for both acoustically unforced and forced conditions. The injectors employed liquid rocket engine relevant propellants of gaseous hydrogen and liquid oxygen. High-speed shadowgraph images along with OH* chemiluminescence captured the hydrodynamic instabilities for each injector and the flame interactions. Overlapping OH* chemiluminescence on top of the shadowgraph images, similar vortex/flame interactions were observed as were observed for a single jet for each individual jet from the injector. Spectral analysis on the OH* chemiluminescence in the near field shows that the individual flames share similar frequency fluctuations when the multi-element array was not subjected to acoustic forcing. These frequencies were also present in the dynamic mode decomposition of the shadowgraph and OH* chemiluminescence images used to investigate the modal structures of both the LOX jet and flame, respectively. Under acoustic forcing, the modal structures of both the LOX jet and flame are the same from each injector.

INTRODUCTION

Liquid rocket engines have been plagued with high frequency combustion instability from their inception [1]. Combustion instabilities in liquid rocket engines arise from complex interactions of acoustic waves coupling and causing oscillatory fluctuation of the volumetric heat release from the combustion process. Combustion instabilities can couple with the combustion chamber acoustics that can directly influence propellant atomization, mixing, flame interactions, and thus, heat release. Combustion instabilities can otherwise also be injector-coupled, where the acoustics from the chamber, propellant feed lines, or injector design drive mass-flow variations into the combustion chamber, causing periodic heat release and pressure fluctuations within the combustion chamber. The complexity of combustion instabilities, and the several potential origins from which they can arise, has usually required expensive trial and error testing to mitigate the severity of the instability in developing new engines [2]. Current efforts in predicting and designing future liquid rocket engines are being developed with computationally expensive models and validating them by using sub-scale liquid rocket engine experiments. This is a more favorable approach since it can potentially limit the amount of expensive development testing. In this effort, a detailed physical and dynamical understanding of the reacting flow from multiple injectors operating at the extreme liquid rocket engine environment is being sought.

Early experiments into understanding combustion instabilities have been documented progressively throughout the years [1-9], and so only the most recent research efforts are reviewed here. The current experimental efforts aimed at studying combustion instabilities are performed by constructing sub-scale combustion chambers that are naturally unstable [10-12] or by the actively driving the reacting forcing with flow modulation [13-15] or speakers. Less extensively investigated is how a single injector's reacting flow field responds physically and dynamically in the presence of neighboring injectors. The few academic studies that have tried are limited in scope to measurements that are possible at such extreme environments. In those studies where optical access is integrated into the experiment, the results typically consist of species selective emission from the flame and time resolved pressure measurements to deduce acoustic/flame interactions. More limited in these studies are quantitative measurements (e.g. Temperature,

velocity, density field, etc…) and a detailed temporal and spatial observations of how the shear flows from multiple injectors and flames interact under acoustic forcing. All of these are vital for the development of future computer models.

Purdue University [10-12] studies combustion instabilities with naturally unstable combustors. Both the transverse instability combustor and the continuously variable resonance combustor are capable of producing self-sustaining transverse and longitudinal combustion instabilities, respectively. The transverse instability combustor is a rectangular combustion chamber with multiple injectors that is capable of producing high-amplitude 1T-mode instability. This is done by locating gas-centered swirl coaxial injectors on either side of a center injector, which is optically accessible. Using high speed backlit imaging with CH* chemiluminescence, they observed CH* emission from the center injector was impeded when the pressure wave was maximum at the center injector. Comparing CFD results with the experimental CH* chemiluminescence, they observed that locations with the highest heat release corresponded well with an increase in the CH* emission both temporally and spatially. This is also the case with the continuously variable resonance combustor, where the combustion instabilities were driven by changing the oxidixer tube length during experimental runs.

Hardi *et. al*. [13-15] employed flow modulation to study high frequency combustion instabilities. This experimental method produces pressure wave excitation of the acoustic resonance modes of the combustion chamber by periodically blocking the exhaust nozzle using a toothed wheel. The location of the toothed wheel determines if transverse or longitudinal instabilities are created for the experimental setup. Hardi *et. al*. studied flame displacement from a multi-element gaseous hydrogen/liquid oxygen shear coaxial to the pressure waves created by the flow modulation. Using the OH* emission from the flame, they employed a flame tracking technique to observe the flame displacement by a transverse acoustic forcing. They attributed the flame displacement to acoustic forcing is probably due to the displacement of the propellants. Even though they collected back-lit imaging from the experiment, due to the vast amounts of density gradients in the reacting flow, few observation were made on the propellant displacement behavior.

Concurrent computational studies performed by Candel *et al*. [16-20], Juniper *et. al.* [21], Sirignano [22,23] and at Edwards AFRL [24] have focused on matching experimental results with their computational models and identifying flow features and physics that lead to combustion instabilities that are missing from the experimental results. Using large eddy simulations of liquid oxygen with a gaseous fuel (Hydrogen or Methane) Candel *et. al.* studied the effects acoustic forcing had on the flame and liquid oxygen jet geometry. Similar to previous experimental results, the liquid oxygen jet shortened and flattened due to the acoustic forcing. They also observed that depending on the acoustic forcing frequency, the flame would have a flag flapping motion or be displace in a bulk fashion. Juniper *et. al.* studied the stability and sensitivity of a coaxial flow using linear models. This was accomplished by varying time and spatial scales for hydrodynamic response to acoustic forcing. They observed that varying the degree of hydrodynamic instabilities greatly influences the regions of heat release and hence the overall thermo-acoustic instability cycle. Sirignano *et. al.* used linear models to study coaxial diffusion flames with and without acoustic forcing. This method used less costly computations to perform a parametric study on varying flow parameters (e.g. injector dimensions) and to observe trends within the flow field. Using a hybrid RANS/LES formulation, researchers at Edwards AFRL studied coupling between acoustics, hydrodynamics, and heat release of Purdue's continuously variable resonance combustor. They investigated the injector's exit conditions under stable and unstable conditions. The physical interactions of the hydrodynamic response of the injector to the acoustic forcing that led to the unsteady heat release are detailed in [24]. They observed that under unstable conditions, vortex shedding from the injector would carry with it unburned propellants and would react when it encounters the incoming pressure wave.

Recent experimental single element studies from Edwards AFRL [25-26] have highlighted several physical interactions between the hydrodynamics instabilities and acoustic forcing that have been missing from the previous experimental studies. Unlike the naturally unstable combustors or the flow modulated combustors, piezo-sirens are used to acoustically drive the reacting flow. The volume occupied by the reacting flow is kept small relative to the volume of the chamber. This ensures that heat release from the combustion is not allowed to from a feed-back loop and become naturally unstable. This method allows for direct observation of how a varying amplitude levels of acoustic pressure influences the reacting flow from a single shear coaxial injector. Using high speed images with OH* emission to study a gaseous hydrogen/liquid oxygen shear coaxial flame, they detailed the influence that shear layer hydrodynamics have on the downstream flow. They observed that when a vortex is formed on the outer shear layer, the vortex would locally consume the liquid oxygen jet at a rapid rate. Spatially at the same location, there will be an increase in OH* emission, where they argued that the vortex would increase the rate of mixing and hence locally consume the liquid oxygen jet. When the same single element was subjected to acoustic forcing, they observed that the outer shear layer vortices would "lock in" to the acoustic forcing frequency when the forcing amplitude was sufficiently high enough.

Using the same experimental chamber at Edwards AFRL, a three element, linear array of shear coaxial injectors were investigated operating at one condition. The linear injector array was studied with and without acoustic forcing. Using high speed shadowgraph and OH* chemiluminescence, this preliminary investigation focuses on the influence the two neighboring elements have on the center injector. This preliminary study is aimed at identifing the spectral behavior and physical interactions between the acoustics and flow features in the near nozzle region that can influence the center injector. Spectral analysis of OH* emission and dyanmic mode decomposition on the high speed images were performed in order to identify the physical flow features that are influencing behavior of the center injector.

EXPERIMENTAL SETUP

The 3 element linear array of shear coaxial injectors was tested at the Stability Lab's high-pressure, windowed combustion chamber at the Edwards AFRL. Figure 1 shows an assembly drawing of the windowed chamber. The main body of the outer chamber is shown in orange. Mounted on the orange chamber are a total of six windows, consisting of two large 101 mm (4 in) diameter round sapphire windows and four oblong windows angled at 45 degree offsets. The chamber is symmetric about the vertical center plane, so only three of the windows are shown in Figure 1. Only the two (diametrically opposed) round windows were used in this study; the oblong windows were not used. The round windows were used for high speed shadowgraphy and OH* chemiluminescence imaging, described further below. The gaseous hydrogen and liquid oxygen enter settling plenums that feed the linear injector array from the grey flange on top. The combustion gases would exit from the green flange on the bottom. Pressurizing nitrogen is introduced into sides of the combustion chamber, as shown in figure 2, hence the combustion process is not used to pressurize the chamber. On either side of the main chamber are high pressure acoustic channels shown in yellow in figure 1, which are connected to and held at the same pressure as the main chamber. Piezoelectric acoustic drivers are attached internally to the grey flanges on either end. There is no flow in the channels other than the flow induced by the acoustics when they are being operated.

Figure 2 shows a schematic of the internal details of the chamber acoustic channel. The acoustic channel constitutes an inner chamber. The inner chamber is connected to and is at the same pressure as the outer chamber and cannot itself sustain any pressure difference with the outer chamber. It does, however, focus the acoustics and limits hot combustion gases from exiting into the main chamber. The outer chamber and associated pressure-containing windows and window seals are therefore not exposed to potentially damaging high temperature combustion gases. The multi-element injector is located in the center of this inner chamber and at the top. The injector issues into the acoustic channel where two opposed flat windows are used as walls of the acoustic channel for visualization, measuring 76.2 mm (3 in) wide by 41.4 mm (1.63 in) high. Three dynamic pressure transducers are located in the rectangular inner windows to measure acoustic pressure fluctuations, as shown in figure 2. In the vicinity of the multi-element coaxial injector, the inner cross section of the acoustic channel normal to the page is rectangular with 20.5 mm (0.81 in) wide (or 13 inner liquid oxygen injector diameters) and 35.5 mm high. The end-to-end length of the acoustic channel or piezo-siren to piezo-siren is 0.75 m or 473 inner liquid oxygen post diameters. There is a round-to-rectangular transition from the acoustic drivers to the channel, but the transition is far enough away from the multi-element injector to not be of any influence.

The combustion chamber is pressurized using nitrogen gas from the two side inlets (which are shown in Figure 2) and does not rely on the combustion process to provide chamber pressure. This is accomplished by keeping the volume occupied by the flame small compared to the combined volume of the inner and outer chambers. This was done in order to maintain accurate control of the chamber pressure and de-couple any thermo-acoustic interactions. Combustion gases exit the inner chamber through a hole in the bottom of the inner chamber and these gases together with pressurizing gases exit the outer chamber through a metering orifice (not shown) at the bottom of the outer chamber. A mixing fitting at the exit, also not shown, dilutes the combustion gas with the exiting pressurizing gas, so that the metering orifice only experiences relatively cool temperatures.

In addition to the fuel and oxidant and pressurizing nitrogen, a separately controlled nitrogen bleed is introduced through round holes in a face plate surrounding the coaxial injector on the upper wall of the inner chamber. The bleed suppresses the formation of a hot gas recirculation zone near the injector that can otherwise influence the

dynamics of the reacting flow. The faceplate with the bleed holes is illustrate in Figure 3. The linear array of coaxial injectors are located in the center of the plate. The inner diameter of each liquid oxygen jet is 1.58 mm (0.0625in), with a LOX post thickness of 0.39 mm. The outer diameter of the hydrogen flow is 2.82 mm (0.11in). The center of each coaxial injector are separated 2.8 inner liquid oxygen diameters away from each other. The diameter of the bleed holes is 0.5 mm. The nitrogen bleed is regulated to a velocity of 0.08 m/s. Also in the faceplate are slots next to the windows for window cooling. In order to avoid steam condensation that would otherwise obstruct the optical view to the reacting flow, the window cooling was also fed gas nitrogen fed with an exit velocity of 5.7 m/s. Although, the velocity from the window purge is high, the momentum flux ratio from the linear injector when compared to the bleed port and the window cooling is well over 10^4 and 15, respectively. Hence, the flow at least in the near nozzle region, the linear injector flow is expected to dominate the downstream flow.

The bleed ports and window cooling manifolds were analyzed to determine the possible presence of resonances that might affect the dynamic results reported in this paper. The resonant frequencies were found to be many times lower than the frequencies associated with these results. The gas circuit of the annular fuel manifold (hydrogen) was similarly analyzed and also found not to be acoustically active for these experiments.

All flows were regulated and metered as high pressure gases and calibrated orifices. Following regulation and metering, the flows were subsequently chilled to the desired temperatures, for example to liquefy the oxygen, using heat exchangers cooled with liquid nitrogen. The pressurizing nitrogen gas and the other nitrogen flows were heated to 305 K to overcome the chilling effects due to Joule-Thompson expansion effects. Each element of the linear injector was designed to have straight passages resulting in fully developed flows at the exit. The internal passages for the linear injector was designed to have injector length to exit diameter (L/D) of over 100. The Reynolds numbers of the fuel and oxygen exceeded 10^4 and are assumed to be turbulent. The pressure and temperature for both LOX and hydrogen were measured before entering the injector. The LOX jet was kept at 140 K, and the hydrogen gas was chilled to 295 K prior to entering the injector. Some heat exchange occurred inside the injector internal passages due to the temperature difference. In order to minimize this heat exchange, the injector was pre-chilled. Before the hydrogen and LOX entered the injector, chilled gaseous nitrogen ran through the hydrogen circuit and liquid nitrogen ran through the LOX fed circuit for 30 minutes prior to combustion.

The chamber pressure used this study was 3.4 MPa (500 psia). This is considerably below the critical pressure of oxygen, so the oxygen was initially a liquid. When the acoustics were present a standing wave was formed at a frequency of 2750 Hz with a wavelength of 0.13 m, which is much larger than the diameter of the injector. The phase of the standing wave was adjusted to correspond to a pressure node at the injector exit. To form the standing wave, a waveform generator, Keysight 33500B, was used to driven high voltage amplifiers, Trek PZD2000A, connected to individual piezo-sirens. A constant pressure amplitude of 13.78 kPa (2 Psi) was used for this study. The pressure amplitude and phase of the standing wave were measured and adjusted using differential pressure transducers, Kulite XCL-100D, prior to ignition. Igniting the flows at this pressure proved to be non-trivial as most spark ignition methods do not work when a high pressure is established prior to ignition as in this experiment. The approach used was a hydrogen-air torch, ignited using a photoignition technique. See Badkahshan et al [27] for details about the photoignition technique.

The reacting flow was visualized with simultaneous high speed shadowgraphy and OH* chemiluminescence. The imaging arrangement is illustrated in Figure 4. The imaging systems captured the unsteadiness of the reacting flow at a framing rate of 25 kHz for 5000 frames or 0.2seconds. The high speed shadowgraph optics were composed of a 7.6cm (3 inch) collimated light source, formed with a ThorLabs SL S202 broadband light source and a spherical 152 mm lens, imaged onto a Phantom Research v 710 with an Sigma Hyperzoom lens. Simultaneously, OH* chemiluminescence was captured with Lambert Instruments HICATT imaged directly onto a Phantom Research v1210 camera. An UV lens (F/2.8 Cerco 2178) with a Semrock (PN FF02-320/40) optical filter were used to image the OH* emission at 308nm. Both cameras have a setup to have a resolution of 0.08mm/pixel. An IRIG time signal synchronized the high-speed imaging and data acquisition systems. A dichroic mirror was used to reflect the UV OH* emission from the flame onto the intensifier, while allowing the visible light to pass through for the shadowgraph images. The both imaging systems captured the over 14 liquid oxygen diameters from the nozzle exit.

The gas-to-liquid momentum flux ratio $\left(J = \frac{\rho U_{Gas}^2}{\rho U_{Liquid}^2}\right)$ has been identified as a global parameter that controls the atomization and breakup a liquid jet in two phase coaxial flows [28]. From previous researchers, it has been observed that if the momentum ratio is too high, then the center liquid is severely shorten and the dynamics and flow physics downstream are highly turbulent and difficult to analyze. In order to understand the impact that neighboring injector's shear layers have on the center injector, a momentum ratio hydrogen to liquid oxygen of 0.5 was selected for this preliminary study.

RESULTS

A sequential series of the instantaneous shadowgraph and OH* emission images is shown in figure 5. In figure 5 the shadowgraph is wavelet fused (left columns) and overlaid (right columns) with its corresponding false colored OH* image. Present in the background of these images are many density gradients from the reacting flow, making it difficult to visualize the hydrogen jet emanating from the linear injector array. Although, the hydrogen jet is difficult to observe, the liquid oxygen jet is clearly visible. From figure 5, each flame envelopes the liquid oxygen jet in the near nozzle region and does not interact with the neighbor until further downstream. In the results observed by Roa *et. al.*[25] for a single injector and using the same propellants, bands of high intensity OH* emission were observed. When the hydrogen jet rolled up into a vortex, it would locally consume the liquid oxygen jet and form a crest on the liquid column. Similar high intensity OH* emission bands are observed in figure 5 for each flame, along with the crests on the liquid oxygen jet.

One way that the center flame can be influenced by its neighbors is through these hydrogen vortex shedding events. As stated earlier, the exact shedding event is difficult to observed directly due to the all density gradients in the background, but the high intensity OH* emission bands, which indicate the presence of an outer shear layer hydrogen vortex, can be tracked for each jet. This can be seen indirectly by tracking the OH* emission fluctuations along a given position of the flame. In figure 5, the interrogation area used to record the OH* emission fluctuations is shown in the green boxes for the left, middle, and right jet flames, for which for now on will be referred to as Jet1, Jet 2, and Jet 3, respectively. The interrogation area is chosen to be one inner liquid oxygen jet diameter away from the nozzle exit and half an inner liquid oxygen diameter in length. Within the interrogation area the OH* emission was integrated for each frame with the temporal mean subtracted. Using a cross spectral density calculation, the OH* emission fluctuations signal of Jet 2 (central injector element or the study element) can be compared with those of the other two.

Figure 6 shows the cross spectral density (CPSD) plots of Jet 2 analyzed with Jet 1 and Jet 3. From the CSPD plots, the frequency with the highest spectral energy among all three jets are close, with 2637 Hz between Jet 2 and Jet 1 and 2647 Hz between Jet 2 and Jet 3. Examining the phase difference from the CPSD plots, the OH* emission fluctuations from the central jet is almost out of phase with its neighboring flames. The phase difference, in degrees, between Jet 2 and 1 is 154˚ and 170.5˚ between Jet 2 and 3. This phase differences corresponds to a time lag of 0.16 milliseconds between Jet 2 and 1 and 0.18 milliseconds between Jet 2 and 3. This indicates that in the near nozzle region, within one inner liquid oxygen diameter, the Jet 2 flame is interacting and being influenced by its neighbors. Specifically, Jet 2 flame's fluctuations are on average out of phase with respect to Jet 1 and 3.

Further investigating the out of phase relationship that the Jet 2 has with its neighbors, dynamic mode decomposition (DMD) was applied on both OH* emission and shadowgraph images. Dynamic mode decomposition is a numerical procedure for extracting dynamical features from flow data. In the DMD applied in this study, the high speed images were decomposed into spatial modes, with each spatial mode having a unique frequency and amplitude. These spatial modes are associated with physical features of the flow field oscillating at a fixed frequency [29]. The larger the mode amplitude of the associated spatial mode, the more dominant that spatial feature is to the flow field being interrogated. The window of interrogation for the DMD analysis for the OH* emission and shadowgraph started at the nozzle exit and extended 5.8 inner liquid oxygen diameters and 10 inner liquid oxygen diameters, respectively. The interrogation area is shown in figure 5. The difference in the interrogation areas is because it assumed that if one hydrogen jet sheds a vortex close to the nozzle, it produces a flow disturbance downstream, causing the other two jets to also shed a vortex lagging the initial vortex. This leads to a convective instability that can manifest itself as the crest on the liquid oxygen jets traveling downstream, due to the flame/vortex interactions previously detailed by Roa *et. al.* The power spectral density of the OH* emission of Jet 2 is shown in figure 7. Plotted on the power spectral density is a shaded region with the frequencies associated with 25% of the total energy from the OH* emission fluctuations.

Comparing this frequency range to the DMD amplitudes, a cluster of DMD amplitude peaks are observed to fall within this frequency range, as shown in figure 8.

Analyzing the spatial modes within this frequency range provides information as to how the flame and the liquid oxygen jet are dynamically and spatially behaving. Figure 9 is the spatial mode associated with the max frequency of 2635 Hz from cross spectral density in figure 7. Figure 9 demonstrates the out of phase relationship Jet 2 has with its neighbors. The alternating red and blue bands in figure 9 are locations where there are changes in OH* emission and surface crests on the liquid oxygen jet. For the OH* emission spatial mode along a fixed distance away from the nozzle, the bands alternate and are nicely organized and degrade the further downstream. This is representative of how the almost 180˚ phase between the jet flame is manifested itself spatially. What is physically occurring is when one hydrogen vortex sheds and produces an OH* emission band across the jet, the other two jet flames response likewise at an almost constant time lag. A comparable offset is present on the shadowgraph spatial mode, but further downstream where the crests on the liquid oxygen surface have enough time grow.

The dynamics the spectral features of the linear injector array were also investigated when subjected to acoustic forcing for the same condition investigated earlier. The linear array was subjected to an acoustic standing wave at a frequency of 2750 Hz and a pressure amplitude of 13.78 kPa (2 Psi). The phase of the standing wave was adjusted so the injector array would be subjected to pressure-node forcing. In a pressure-node the velocity fluctuations are maximum, hence the injector array was subjected to an oscillating velocity field. Figure 10 shows instantaneous images of the reacting flow subjected to acoustic forcing. The liquid oxygen jet is drastically different compared to the unforced case in figure 5. From figure 10 the liquid oxygen jet has developed periodic lobes. The flame also takes on a similar shape near the nozzle exit with high intensity OH* emission located between the lobes of the liquid oxygen jet. It was shown previously [26] that when a single coaxial jet is subjected to pressure-node forcing, the jet takes on an S-shape. This S-shape is consistent in Jets 1, 2, and 3, with the lobes on individual liquid oxygen jets being slanted.

Theoretically, when these types of flows are subjected to a transverse acoustic velocity, this causes improved mixing of the propellants. What occurs is that with each passing acoustic wave, propellants are transported or displaced. This displacement brings unreacted fuel or oxidizer closer or impinges one on its counterpart, resulting in increased mixing of the propellants. This unreacted mixture then releases its energy in phase with acoustic pressure, forming a feedback loop towards a combustion instability limit cycle. This appears to be occurring for all three flames in this study.

Dynamic mode decomposition of the OH* emission and shadowgraph images when subjected to pressure node forcing shows the flame and its effect on the downstream flow. The DMD analysis was applied at the same locations as the unforced condition, as shown in figure 5. Figure 11 shows the DMD amplitude along with the spatial mode at the forcing frequency 2750 Hz. The DMD amplitude for both set of images shows strong frequency peaks at the forcing frequency along with higher harmonics, indicating the flow field has strongly coupled with the acoustic forcing. The DMD spatial mode for 2750 Hz, shows that the alternating OH* emission pattern is slanted unlike the unforced condition. This slanted alternating pattern is representative of changes in OH* emission intensity. It is suspected that as the transverse velocity field pushes on one side of the hydrogen jet and brings it closer to the liquid oxygen jet. This increases local equivalences ratios on the side that forcing and/or displaced occurs and consumes the liquid oxygen, resulting in the lobes shown in figure 10. The DMD spatial mode from the shadowgraph images shows an offset alternating pattern, representative of the lobes on the liquid oxygen jet. The lobe pattern is observed to fully develop further downstream, hence the displacement of the flame in the near nozzle region influences the shape of the liquid oxygen jet downstream. Given that the physical features of the flame and liquid oxygen jet are the same across linear array, Jet 2 does not seem to be greatly influenced by its neighbors. Instead, all three jets appear to have coupled with the acoustic forcing, minimizing their interactions among each unlike the unforced condition.

CONCLUSION

The reacting flow dynamics from a linear array of three shear coaxial injectors operating under sub-critical pressures was investigated with and without acoustic forcing. High-speed shadowgraph and OH* chemiluminescence mages recorded the center injector's response and behavior under the influence of its neighboring injectors. In the unforced condition, all three jet flames were coupled within a narrow frequency band and were almost completely out of phase with each other. This indicated that when one jet produced a flow disturbance, such as vortex shedding, the other two responsed in kind with a time lag. Dynamic mode decomposition of the unforced condition, showed that the physical features from each jet were indeed out of the phase with each other. When the linear array was subjected to

a transverse acoustic velocity field, all three jets had the same response coupling with the acoustic forcing, with little observed inter-jet interactions. It was observed that in all the jets, the liquid oxygen jet developed altenrating lobes on either side, which was picked up by the DMD analysis. The DMD analysis also revealed that the flame had slanted lobes that is consistent with transverse acoustic field displacing the outer hydrogen jet closer to the liquid oxygen jet. These results elucidate the the flow-flame interactions that occur when driving non-premixed rocket flames by transverse acoustic.

REFERENCES

[1] Ross, C. C., and Datner, P. P., "Combustion Instability in Liquid-Propellant Rocket Motors–A Survey," Selected Combustion Problems, edited by Hawthorne, W. R., Fabri, J., and D. B., Spalding, Butterworths Scientific, London, 1954, pp. 352–380.

[2] Oefelein, J. C., and Yang, V., "Comprehensive Review of Liquid- Propellant Combustion Instabilities in F-1 Engines," Journal of Propulsion and Power, Vol. 9, No. 5, 1993, pp. 657–677.

[3] Anderson, W. E., Ryan, H. M., and Santoro, R. J., "Combustion Instability Phenomena of Importance to Liquid Bi-Propellant Rocket Engine," 28th JANNAF Combustion Subcommittee Meeting, edited by Gannaway, M. T., Chemical Propulsion Information Agency (CPIA), Columbia, MD, 1991, pp. 99–112.

[4] Crocco, L., and Cheng, S.I., Theory of Combustion Instability in Liquid Propellant Rocket Motors, AGARDograph 8, Princeton Univ., Princeton, NJ, 1956, pp. 1–24.

[5] Harrje, D. T., and Reardon, F. H., "Liquid Propellant Rocket Combustion Instability," NASA Special Publ. SP-194, 1972.

[6] Culick, F. E. C., "Combustion Instabilities in Liquid-Fuelled Propulsion Systems," AGARD Conference Proceedings, NATO Paper 450, Neuilly sur Seine, France, 1988.

[7] Culick, F. E. C., "Unsteady Motions in Combustion Chambers for Propulsion Systems,"NATOAGARDograph AG-AVT-039, California Inst. of Technology, Pasadena, CA, 2006.

[8] Yang, V., and Anderson, W. E. (eds.), Liquid Rocket Engine Combustion Instability, Vol. 169, Progress in Astronautics and Aeronautics, AIAA, Washington, D.C., 1995.

[9] Natanzon, M. S., Combustion Instability, Vol. 222, Progress in Astronautics and Aeronautics, AIAA, Washington, D.C., 2008.

[10] Morgan C. J., Shipley, K. J., and Anderson, W. E., "Comparative Evaluation between Experiment and Simulation for a Transverse Instability," Journal of Propulsion and Power, Vol. 31, No. 6, 2015

[11] Pomeroy, B. R., Morgan, C., and Anderson, W. E., "Response of a Gas Centered Swirl Coaxial Injector to Transverse Instabilities," 47th AIAA/ ASME/SAE/ASEE Joint Propulsion Conference & Exhibit, AIAA Paper 2011-5698, 2011

[12] Yu. Y. C., Sisco, J. C., Rosen, S., Madhav, A., and Anderson W. E., "Spontaneous Longitudinal Combustion Instability in a Continuously Variable Resonance Combustor," Journal of Propulsion and Power, Vol. 28, No.5, 2012

[13] Hardi. J. S., Beinke, S. K., Oschwald, M.., and Dally, B. B., "Coupling of Cryogenic Oxygen-Hydrogen Flames to Longitudinal and Traverse Acoustic Instabilities," Journal of Propulsion and Power, Vol. 30, No. 4, 2014

[14] Gröning, S., Hardi. J. S., Suslov. D., and Oschwald. M., "Injector-Driven Combustion Instabilities in a Hydrogen/Oxygen Rocket Combustor," Journal of Propulsion and Power, Vol. 32, No. 3, 2016

[15] Hardi. J. S., Oschwald. M., and Dally, B. B., “Study of Lox/H2 Spray Flame Response to Acoustic Exictation in a Rectangular Rocket Combustor,” 49th AIAA/ ASME/SAE/ASEE Joint Propulsion Conference & Exhibit, AIAA Paper 2013-3781, 2013

[16] Hakim. L., Schmitt. T., Ducruix, S., and Candel S., “Dynamics of a Transcritical Coaxial Flame under High-Frequency Transverse Forcing: Influence of the Modulation Frequency on the Flame Response,” Combustion and Flame, 162, 2015

[17] Urbano, A., Selle, L., Staffelbach, G., Cuenot, B., Schmitt, T., Ducruix, S., and Candel, S., “Exploration of Combustion Instability Triggering using Large Eddy Simulation of a Multiple Injector Liquid Rocket Engine,” Combustion and Flame, 169, 2016

[18] Richecoeur, F., Ducriox, S., Scouflaire, P., and Candel, S., “Experimental Investigation on High-Frequency Combustion Instabilities in Liquid Rocket Engines,” Acta Astronautica, 62, 2008

[19] Rey, C., Ducruix, S., Richecoeur, F., Scouflaire, P., Vingert, L., and Candel, S., “High Frequency Combustion Instabilities Associated with Collective Interactions in Liquid Propulsion,” 40th AIAA/ ASME/SAE/ASEE Joint Propulsion Conference & Exhibit, AIAA Paper 2004-3518, 2004

[20] Richecoeur, F., Scouflaire, P., Ducruix, S., and Candel, S., “High-Frequency Transverse Acoustic Coupling in a Multiple-Injector Cryogenic Combustor,” Journal of Propulsion and Power, Vol. 22, No. 4, 2006

[21] Magri. L., See, Y. C., Tammisola, O., Ihme, M., and Juniper, M. P., “Multiple-Scale Thermo-Acoustic Stability Analysis of a Coaxial Jet,” Proceedings of the Combustion Institute, 36, 2017

[22] Popov, P. P., Sideris, A., and Sirignano, W. A., “Low-Probability Events Leading to Rocket Engine Combustion Instability,” Journal of Propulsion and Power, Vol. 55, No. 3, 2017

[23] Sirignano, W. A., and Krieg, J., “Coaxial Jet Flame Subject to Long-Wavelength Acoustic Oscillations,” Journal of Propulsion and Power, Vol. 32, No. 3, 2016

[24] Harvazinski, M. E., Huang, C., Sankaran, V., Feldman, T. W., Anderson, W. E., Merkle, C. L., and Talley, D. G., “Coupling Between Hydrodynamics, Acoustics, and Heat Release in a Self-Excited Unstable Combustor,” Physics of Fluids, 27, 2015

[25] Roa, M., and Talley, D. G., “Vortex Dynamic Mechanisms in Coaxial in Hydrogen/LOX Jet Flames,” Submitted to Journal of Propulsion and Power, 2018

[26] Roa, M., Forliti, D., Badakhshan, A., and Talley, D. G., “Acoustically Forced Coaxial Hydrogen/ Liquid Oxygen Flames,” ILASS Americas 28th Annual Conference, 2016

[27] Badakshan, A., and Danczyk, S., “Ignition of Nanoparticles by a Compact Camera Flash,” DTIC http://www.dtic.mil/dtic/tr/fulltext/u2/a614547.pdf

[28] Marinet, M. F., and Schettini, E. B. C.,“The density field of coaxial jets with large velocity ratio and large density differences,” International Journal of Heat and Mass Transfer, Vol. 44, 2001

[29] Schmid, P. J., “Dynamic Mode Decomposition of Numerical and Experimental Data,” Journal of Fluid Mechanics, Vol 656, 2010

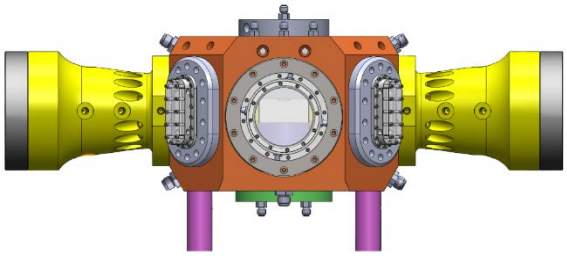

Figure 1. Assembly drawing of the combustion chamber.

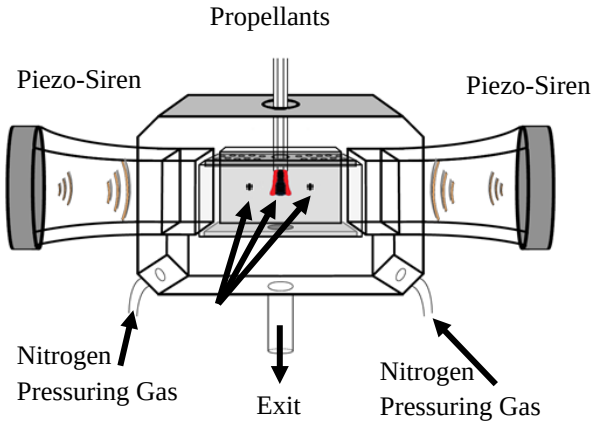

Figure 2. Inner details of the combustion chamber. P' is the location of the differential pressure transducers. The gray section in the middle is the optical windows used to complete the acoustic channel.

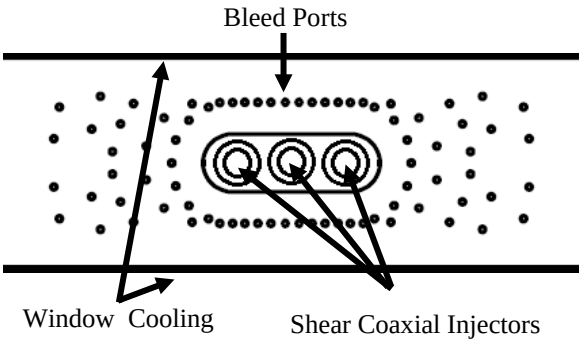

Figure 3. The injector faceplate with bleed ports, window film cooling, and linear array injector in the center.

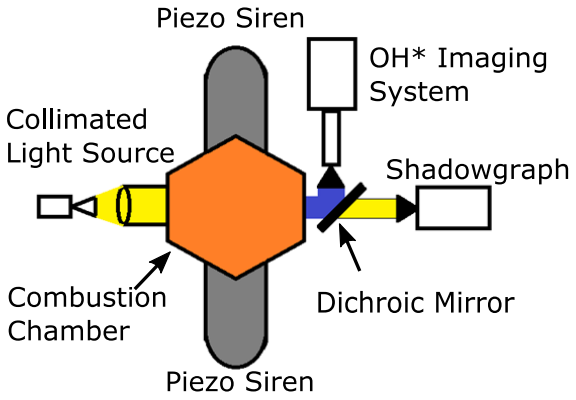

Figure 4. High speed, simultaneous imaging system layout.

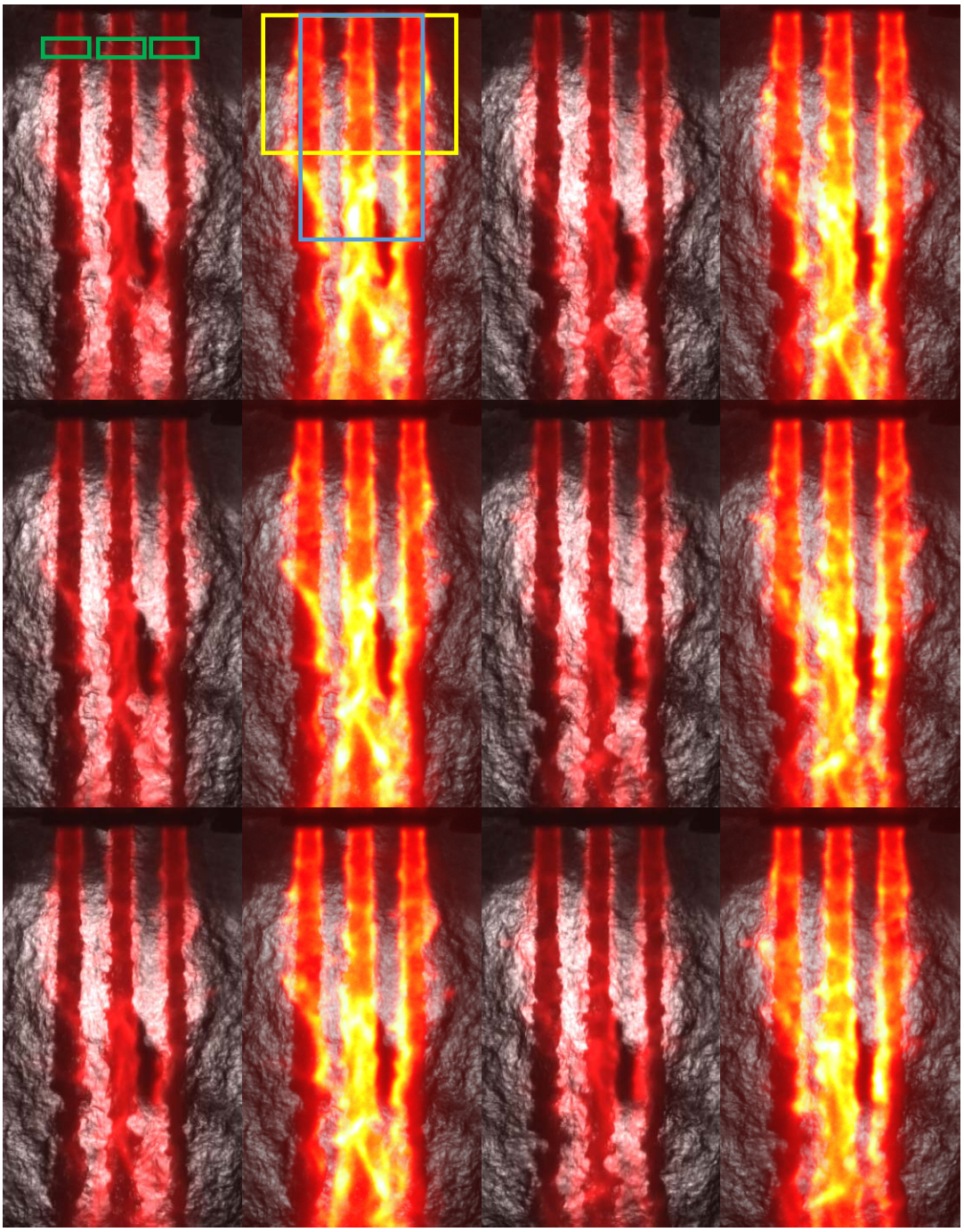

Figure 5. Instantaneous images of the shadowgraph with OH* emission wavelet fused and overlapped (Left column then immediate right, respectively). The time separation between each frame is 0.16 milliseconds. The flame in the near nozzle region don't merge or interact. Each flame surrounds its corresponding liquid oxygen jet. At the locations of high OH* emission, waves form on the liquid oxygen jet. The images are sequential from top to bottom, left to right. The green rectangles are the locations where the OH* emission fluctuations were recorded. The yellow and blue squares is where the DMD snapshots were taken for the OH* emission and shadowgraph, respectively.

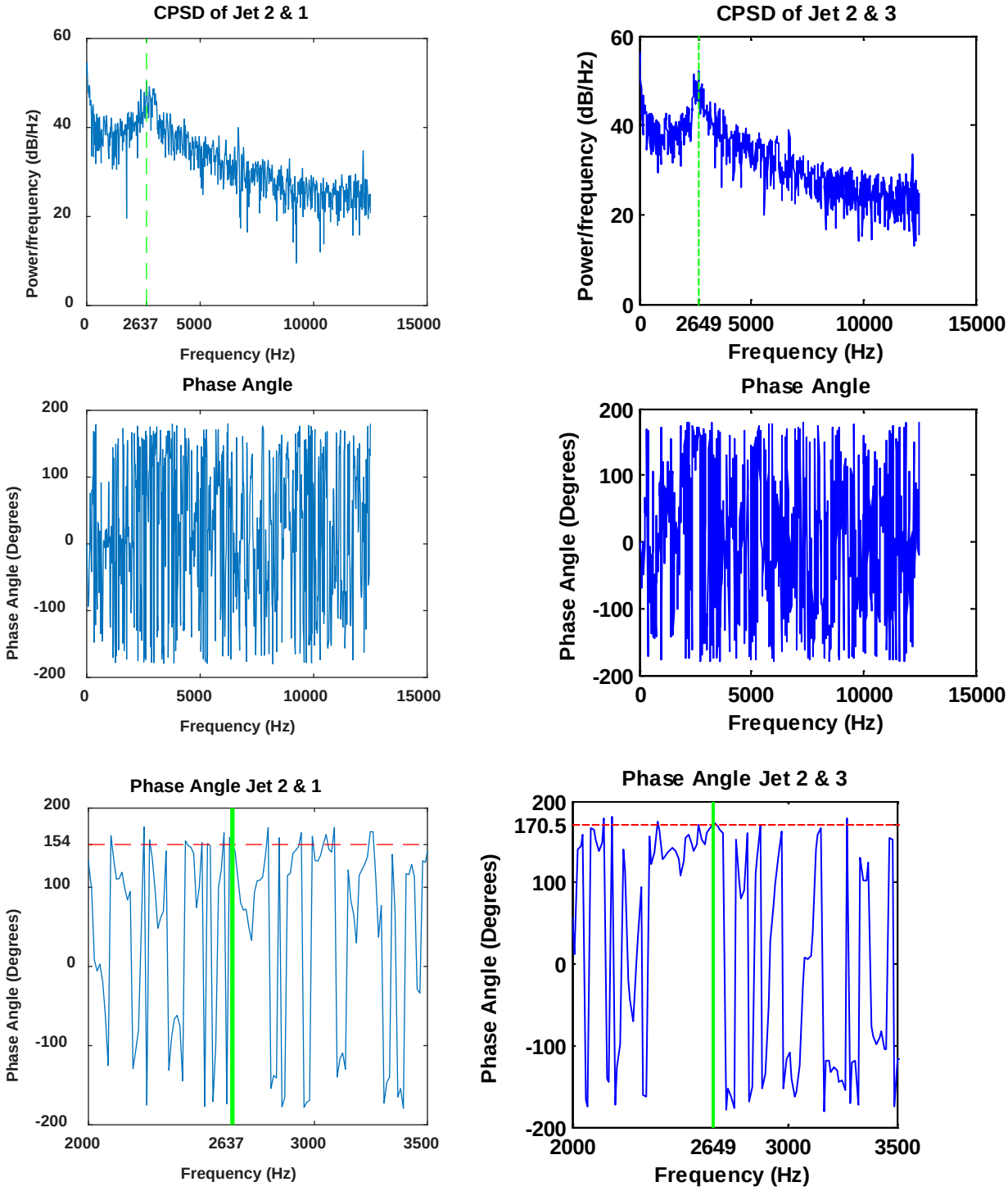

Figure 6 The cross spectral density estimates (CSPD) of the OH* fluctuations between, left column, Jet 2 and Jet 1, and the right column is between Jet 2 and Jet 3. Below each CPSD is the phase between both signals, along with a narrow frequency window. The green line is the dominate frequency and the red dash line is the corresponding phase between both signals.

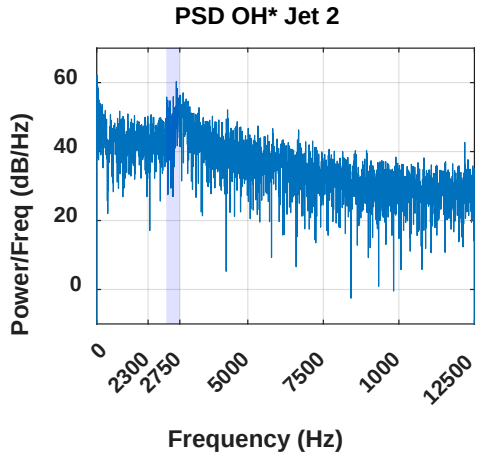

Figure 7. Power spectral density plot of Jet 2, with a shaded region that occupies 25% of the total energy. Between frequencies 2306 and 2756 Hz.

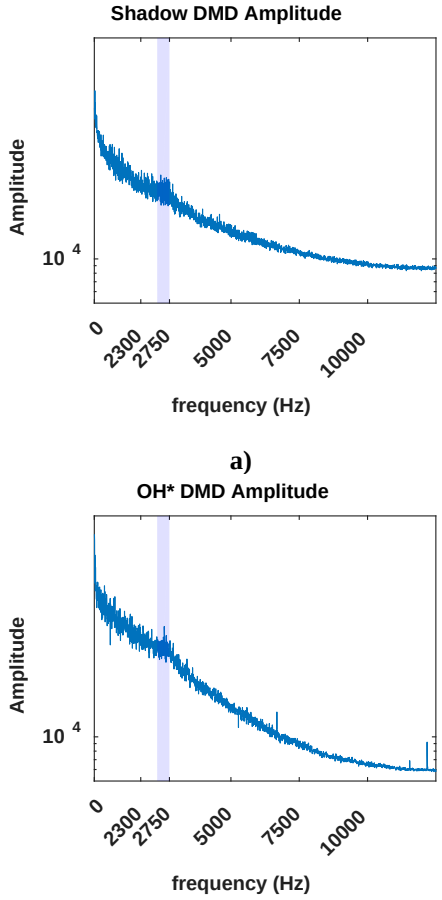

Figure 8. The DMD Mode Amplitude vs Frequency. The shaded region is the 25%occupied frequency from Jet2 for a) Shadowgraph and b) OH* emission.

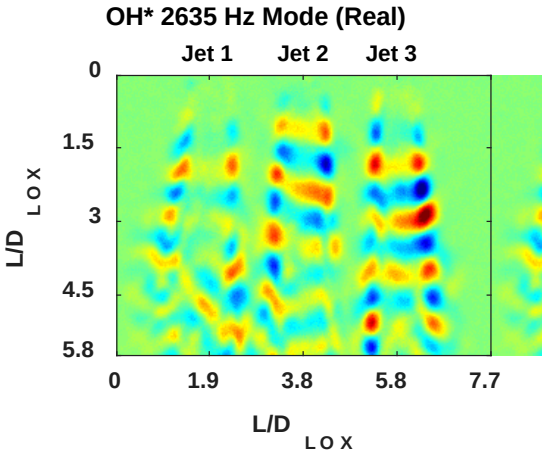

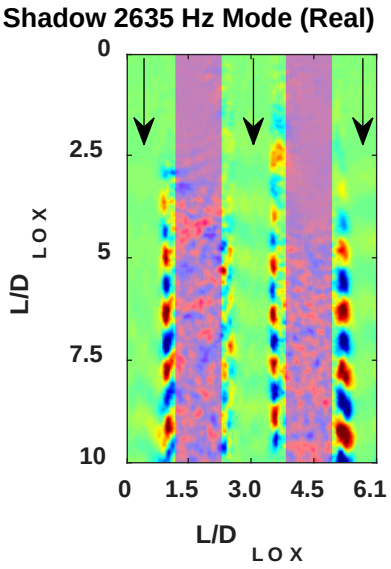

Figure 9. The DMD spatial mode corresponding to the 2635 Hz frequency for: a) OH* emission and b) the shadowgraph. The alternating pattern are indicative of flame shedding events and surface wave on the liquid oxygen surface. The purple is the inter-injector spacing and the arrows point in the direction of the liquid oxygen jet flow.

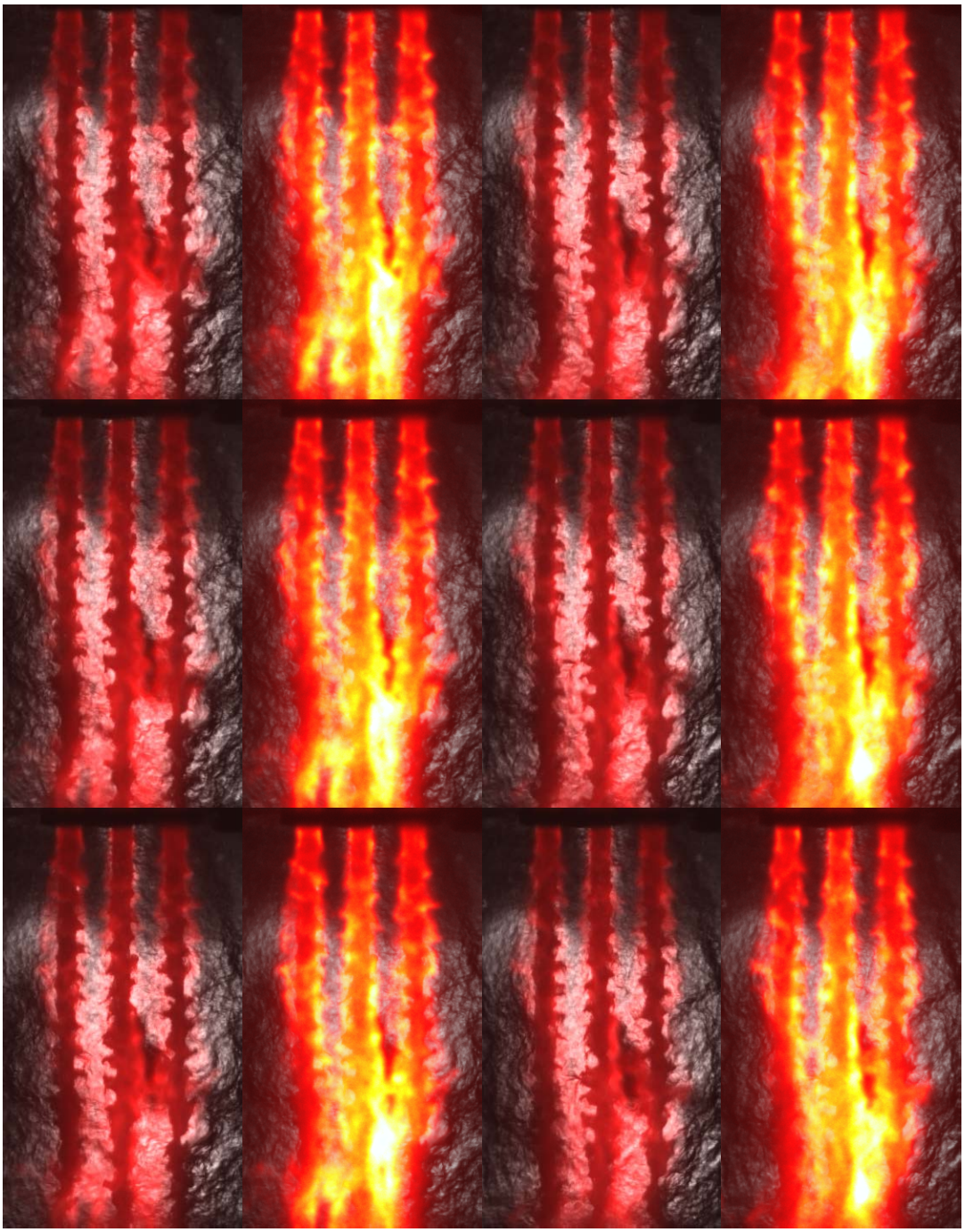

Figure 10 Instantaneous images of the shadowgraph with OH* emission wavelet fused and overlapped (Left column then immediate right, respectively). Subjected to pressure node forcing. The flame still surrounds its liquid oxygen jet in the near nozzle region. All three liquid oxygen jets have developed lobes at the same spatial location where there are high OH* emission. The flame has also take on the lobe shape near the injector exit. The time separation between each frame is 0.16 milliseconds. The images are sequential from top to bottom, left to right.

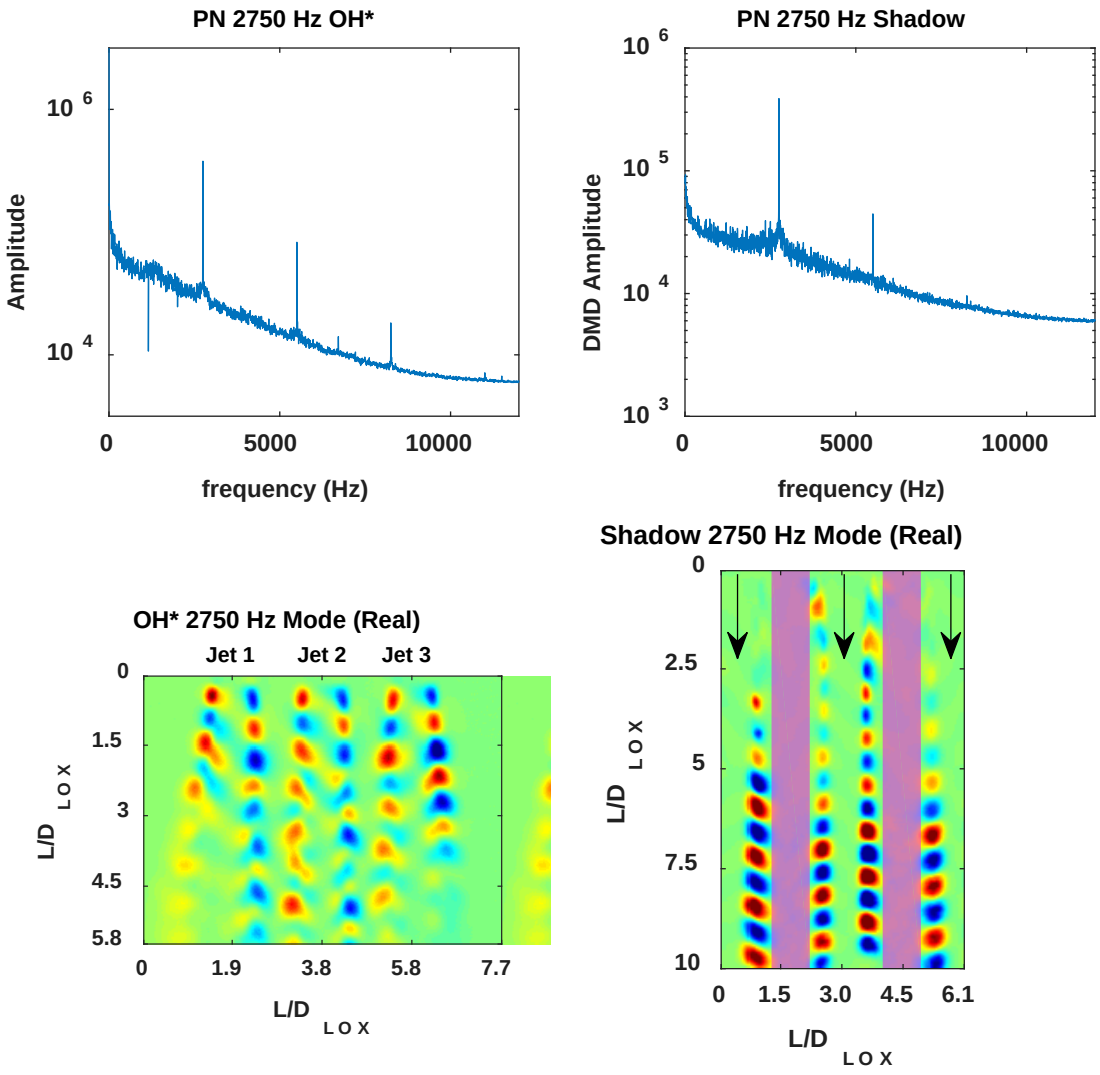

Figure 11. The OH* and shadowgraph DMD amplitude for the acoustic forcing condition at 2750 Hz. The corresponding spatial mode for each shows a slanted lobe pattern and offset alternating pattern for the OH* and shadow graph, respectively. The adjacent shear layers next to Jet 2 are out of phase with each other. The purple is the inter-injector spacing and the arrows point in the direction of the liquid oxygen jet flow.

Integrity ★ Service ★ Excellence

PRELIMINARY STUDY OF THE REACTING FLOW FROM MULTI-ELEMENT SHEAR COAXIAL FLOWS

05 24 2018

Mario Roa, Ctr

Douglas Talley, Cil

RQRC

Air Force Research Laboratory

Objectives

- **Study a 3 element, linear array of shear, coaxial injectors at sub-critical pressures.**

- **Preliminary results are aimed at identifying how the neighboring injectors influence the center injector dynamics and flow features.**
  - **This was done using a dual-camera setup of shadowgraph with OH* chemiluminescence to study the flame and hydrodynamic response of the center injector.**

- **Subject the linear injector a transverse acoustic velocity perturbations and study the inter-element behavior.**

3 Element, Linear Injector Array

Features

- Linear injector array, featuring 3 elements, is shown to the right.
- Liquid oxygen flows through the center with gaseous hydrogen flows on outside.
- The injector housing was 3-D printed.
- The oxygen tubes are concentrically held with tabs printed onto the housing.
- The injectors are 2.88 LOX diameter apart.

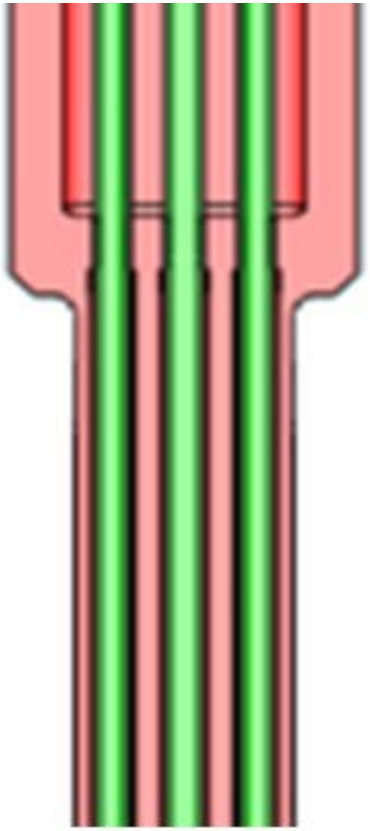

Hydrogen Ø 0.114”
Oxygen Ø 0.062”
Gap 0.010”

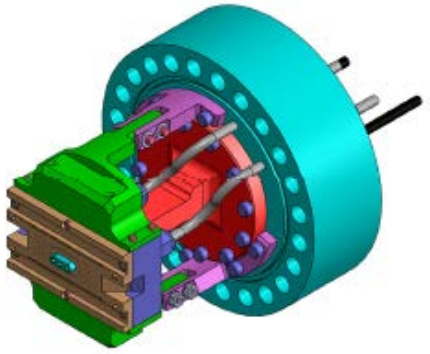

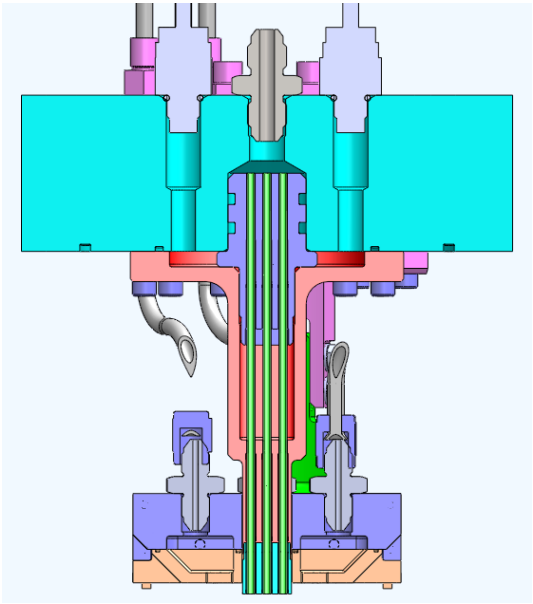

Operating Conditions

- Propellants Cryogenic liquid O_2 and gaseous H_2 flame (With and without acoustics)
  - Pressure node forcing at 13.78 kPa (2 Psi)
- J – 0.5 (Single Condition)
- O_2 inner jet @ 140 K
- H_2 outer jet @ 295 K
- The linear injector is at the center of the face plate.
  - The face has window cooling and bleed ports
  - The bleed ports are used to suppress hot gas recirculation near the injector exit.
- Fully-developed turbulent flow conditions (L/D over 100 for propellants within the injector.)
- Chamber pressure 3.4 MPa (500 psi)→ subcritical
- Optical systems were set at 25kHz or 40µs between each frame.

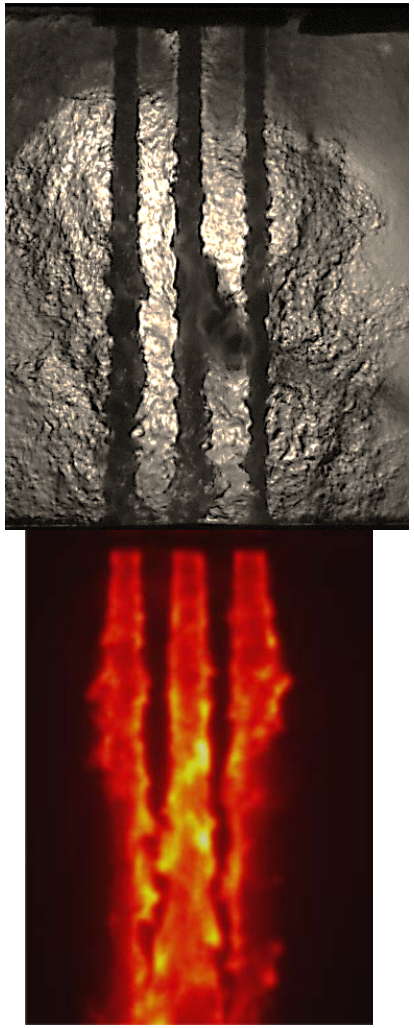

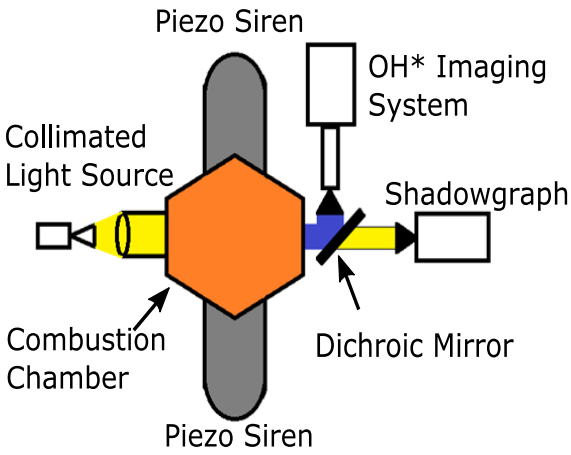

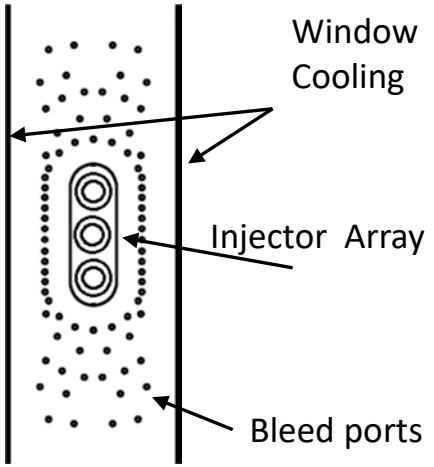

Experimental Facility

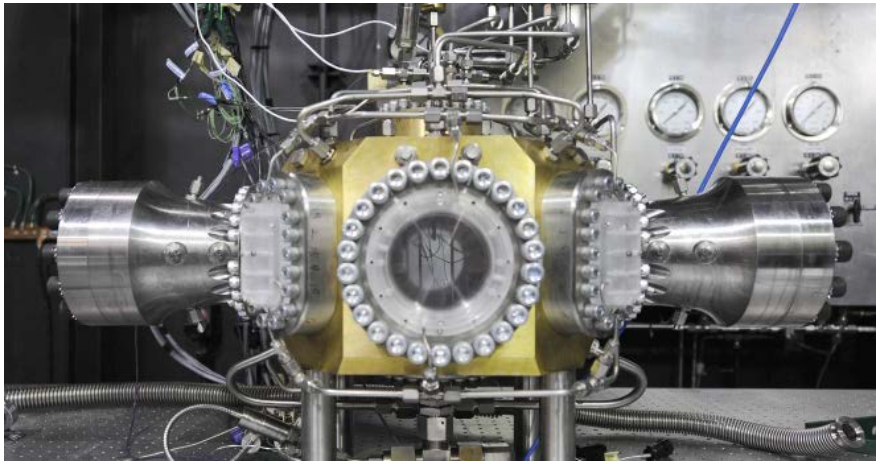

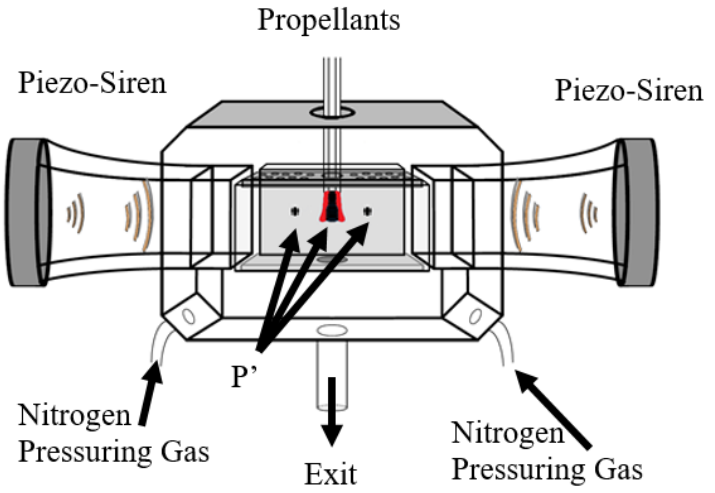

Features

- Frequency and amplitude independent of combustion – accurate control of frequency and amp.
- Pressurization independent of combustion – accurate control of pressure.
  - Subcritical and supercritical pressures
- Precise cryocooler – accurate control of temperature to within ±1 K.
- Chamber-within-a-chamber
  - Outer chamber contains pressure – pressure containing elements remain cool
  - Inner chamber contains acoustics and combustion only – allows finer adjustment of inner elements
- High amplitude piezosirens specially designed for high pressure
- On-axis windows for shadowgraph, Schlieren, chemiluminescence, CH*/OH* emission
- Off-axis windows for PIV/PLIF
- Fully developed turbulent injector flows – well known boundary conditions
- High-speed pressure transducers

Rayleigh Index fields

Unforced Results (J = 0.5)

Shadowgraph

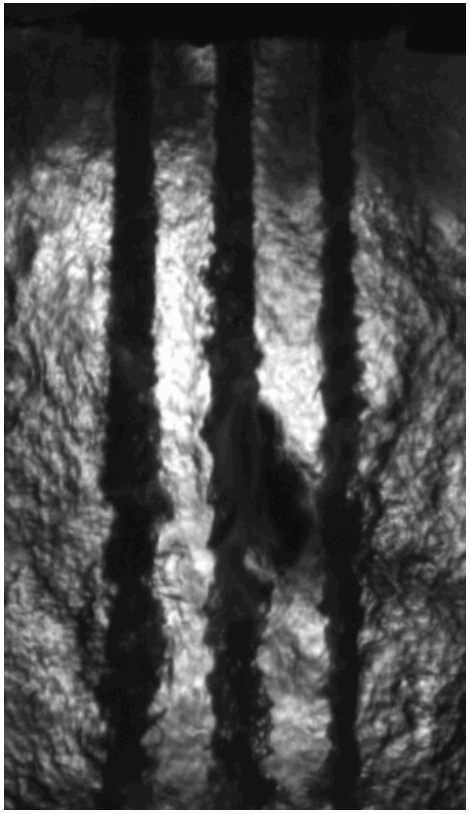

OH*

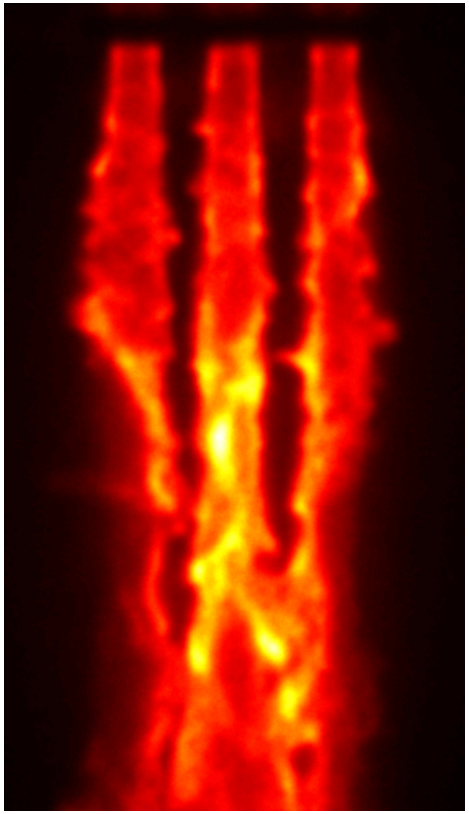

FUSED

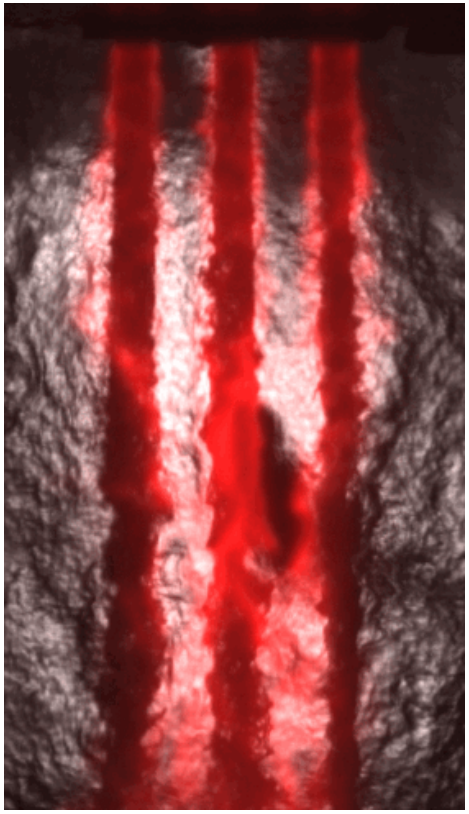

- The background is saturated with density gradients in the shadowgraph.
- Periodic shedding OH* fluctuations are present.
- Flame is attached at the nozzle exit.

OH* Emission Fluctuations

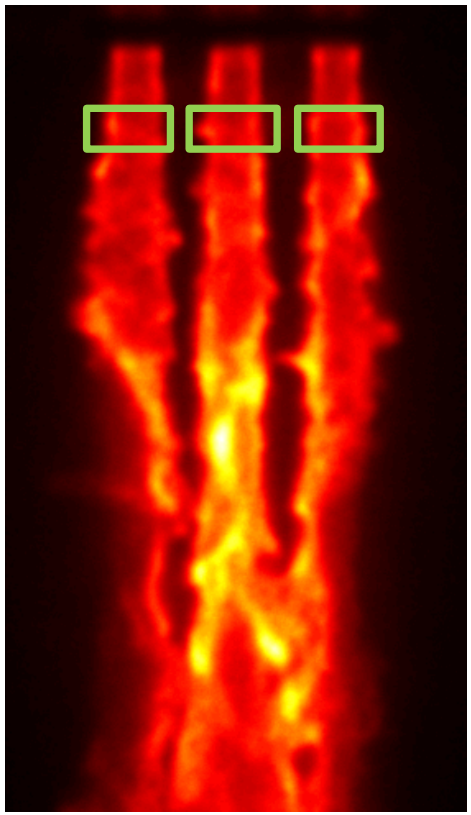

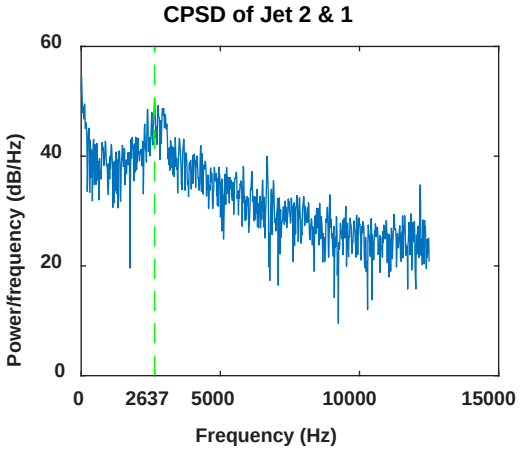

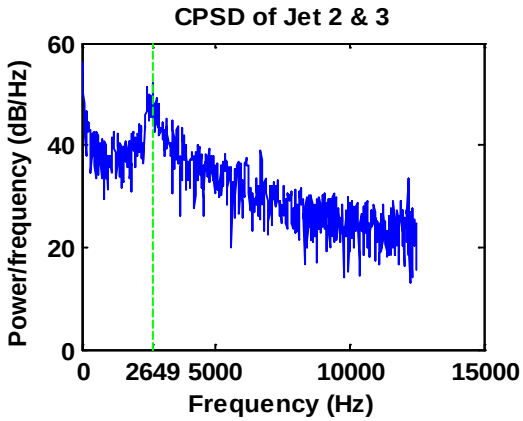

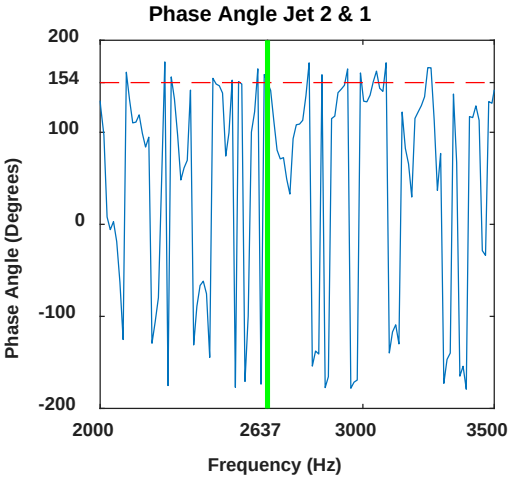

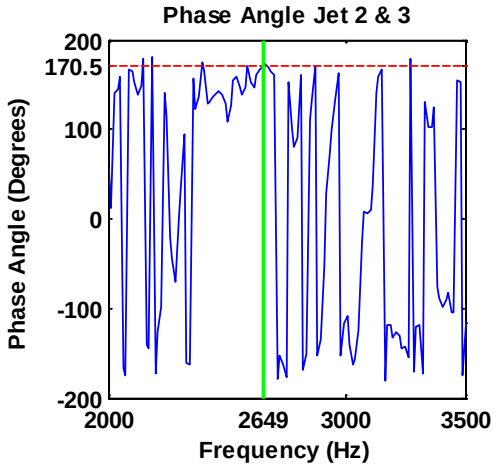

- Share frequency peak around 2635 Hz (Peak of center element).
- OH* emission are out of phase.

Dynamic Mode Decomposition

Extract spectrally-pure temporal modes with detailed spatial mode shapes

- Schmid (2010) and Rowley et al. (2009)
- Employ time-averaged amplitude measurement described by Alenius (2014)
- 5000 samples used

$$I(x,y,t) = \mathrm{Re}\left(\sum_{i=1}^{n} \tilde{A}_i \exp(\tilde{\lambda}_i t) \tilde{D}_i(x,y) \right)$$

Amplitude of mode at t = 0

Accounts for growth of mode in time as well as temporal frequency

Complex spatial mode shape

Properties of DMD

- Isolates response of flow at forcing frequency and harmonics
- Single modes can reconstruct convective processes (POD requires two modes)
- Less efficient at reconstructing signal energy compared to POD

Dynamic Mode Decomposition Analysis

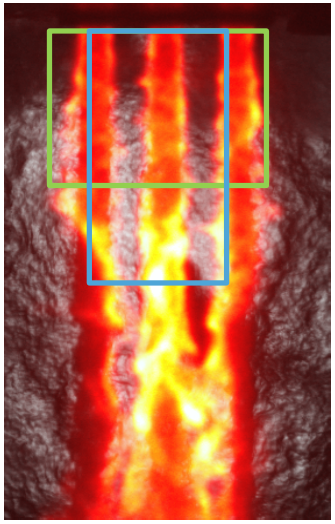

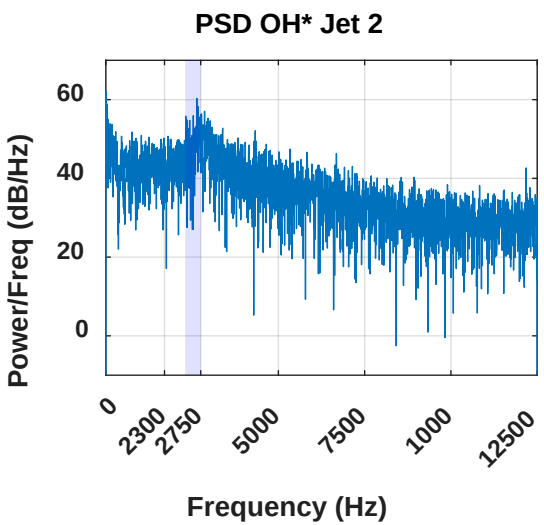

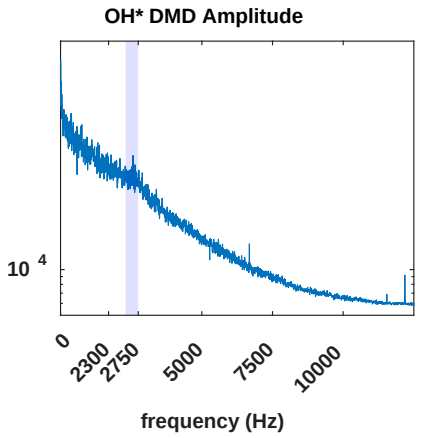

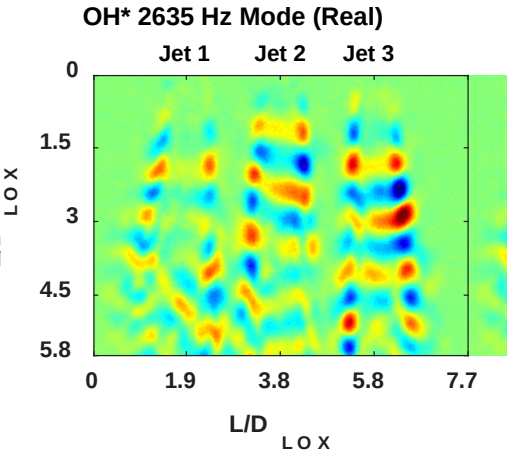

- From Power spectral density of the Jet 2. 25 % of the energy is within 2300 to 2700Hz
- The DMD analysis has similar peaks within that frequency range
- The DMD spatial shows for 2635 Hz mode shows the flow structures are offset (hence out of phase.)

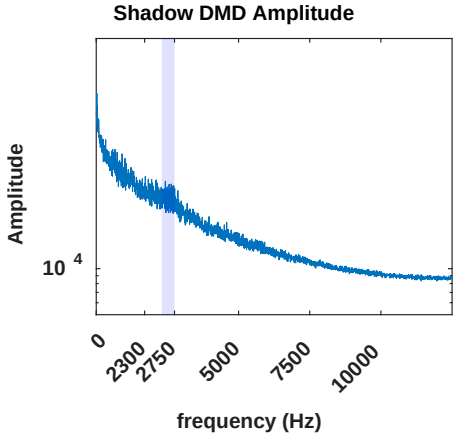

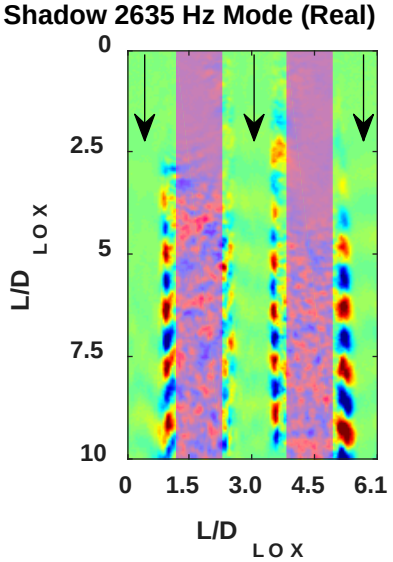

Single Element Dynamics

FUSED | Shadowgraph | OH*

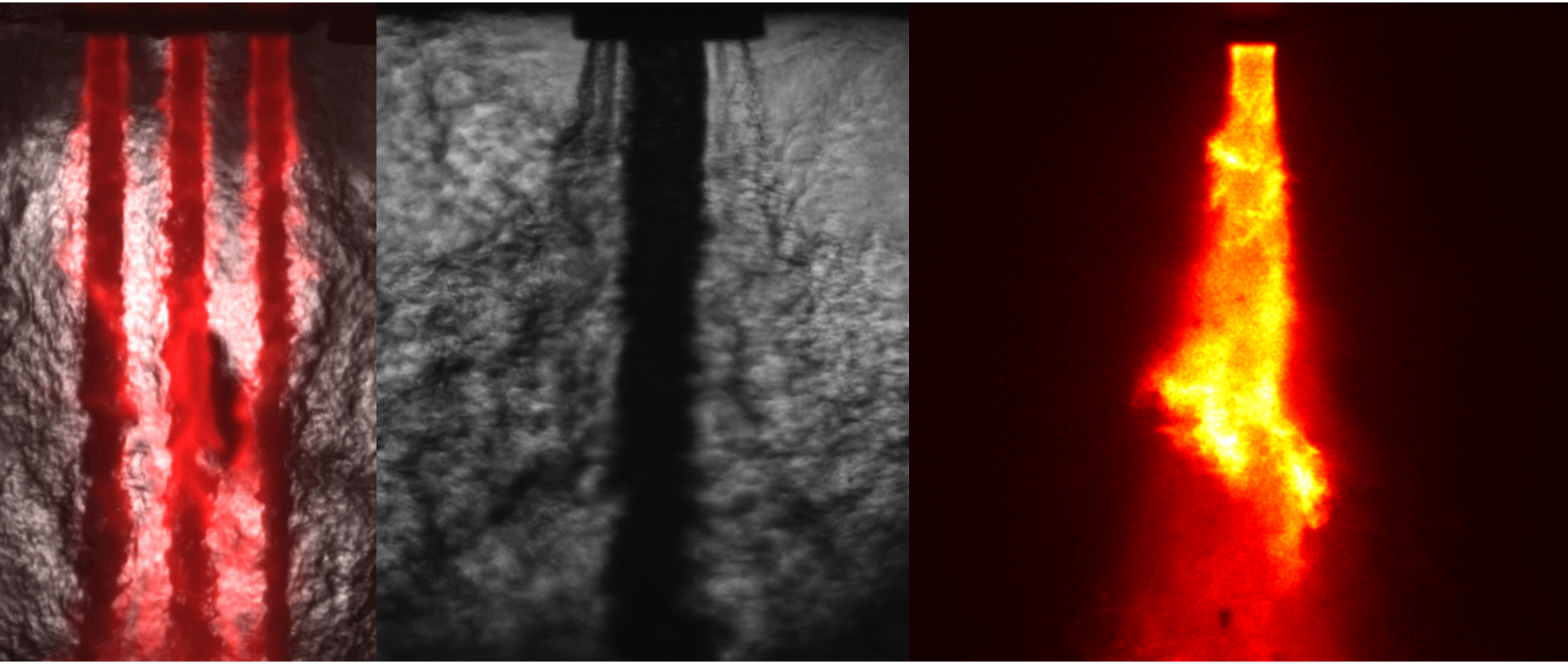

- Zooming in on the outer hydrogen shear layer is shown to be unstable with vortex shedding.
- Single element shows the same periodic shedding OH* fluctuations are present.
- Single elements results have been previously presented.
  (Videos are not at the same framerate or one to one)

Single Element Hydrodynamic Instability

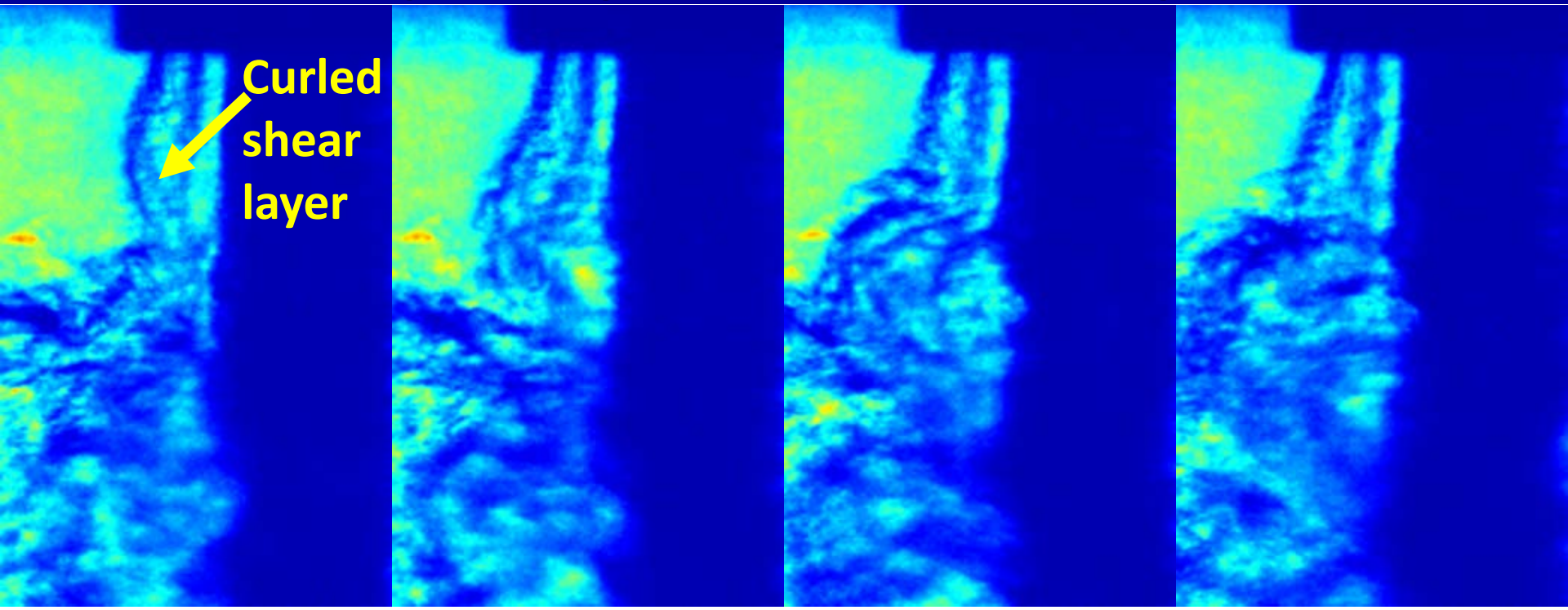

- Sequential shadowgraph images. (False colored shadowgraph images to see the outer hydrogen shear layer.)
- The outer hydrogen shear layer is observed to curl towards the LOX jet.
- At a Δt time later (less than 40μs) a localized increase in OH* emission is observed.
- Afterwards, the outer shear layer is pushed out and then sheds as a vortex.

Hydrodynamic Instability

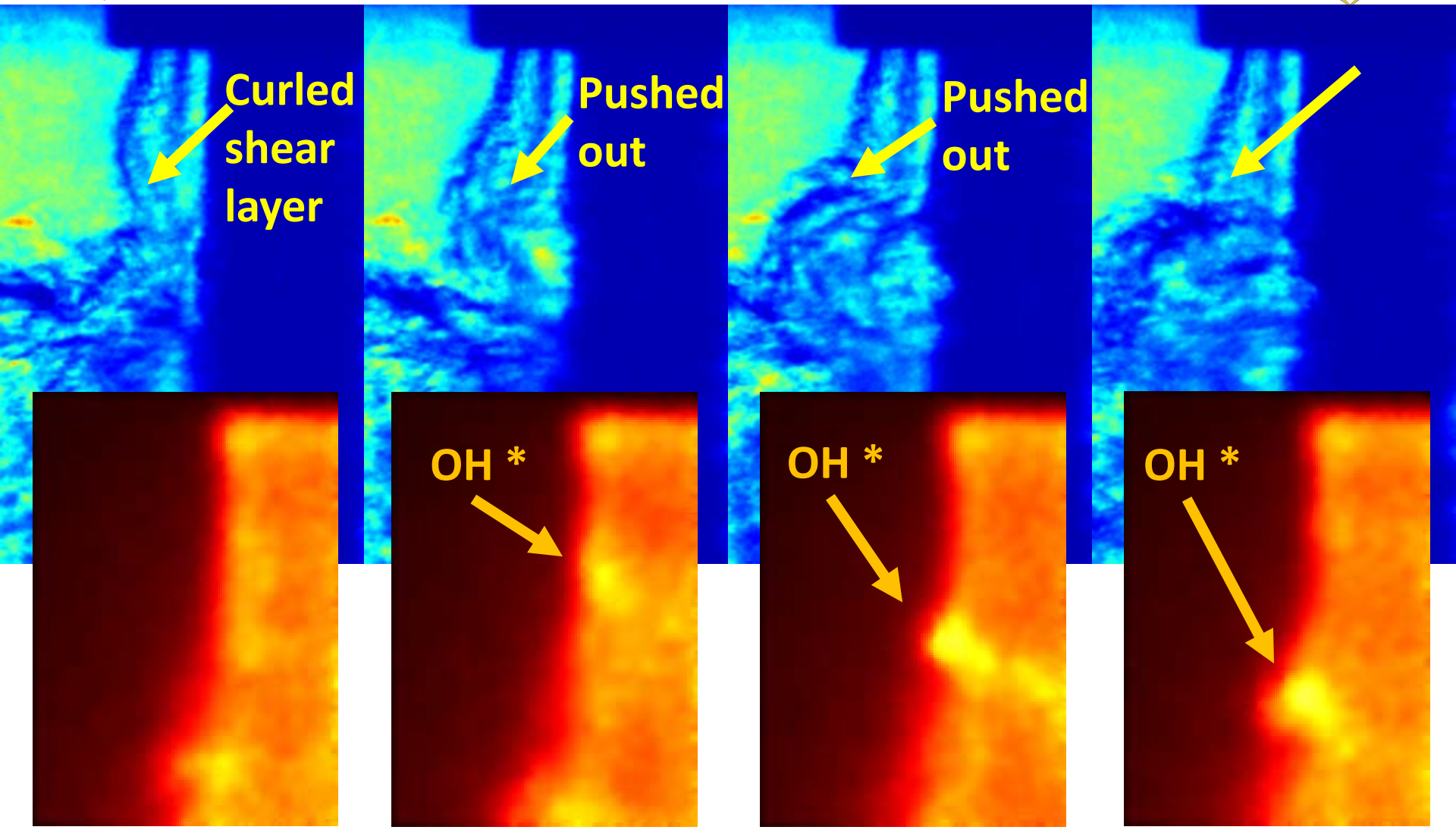

The OH* wave convects downstream and co-annular hydrogen vortex sheds.

OH* Tracking

Jet 1 Jet 2 Jet 3

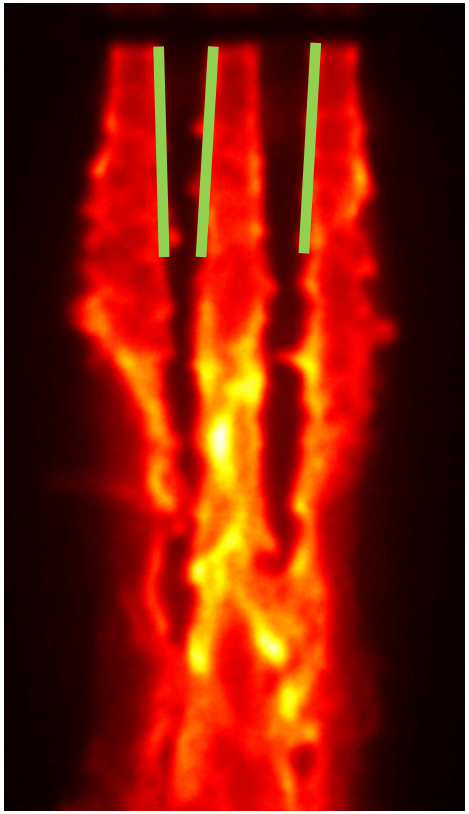

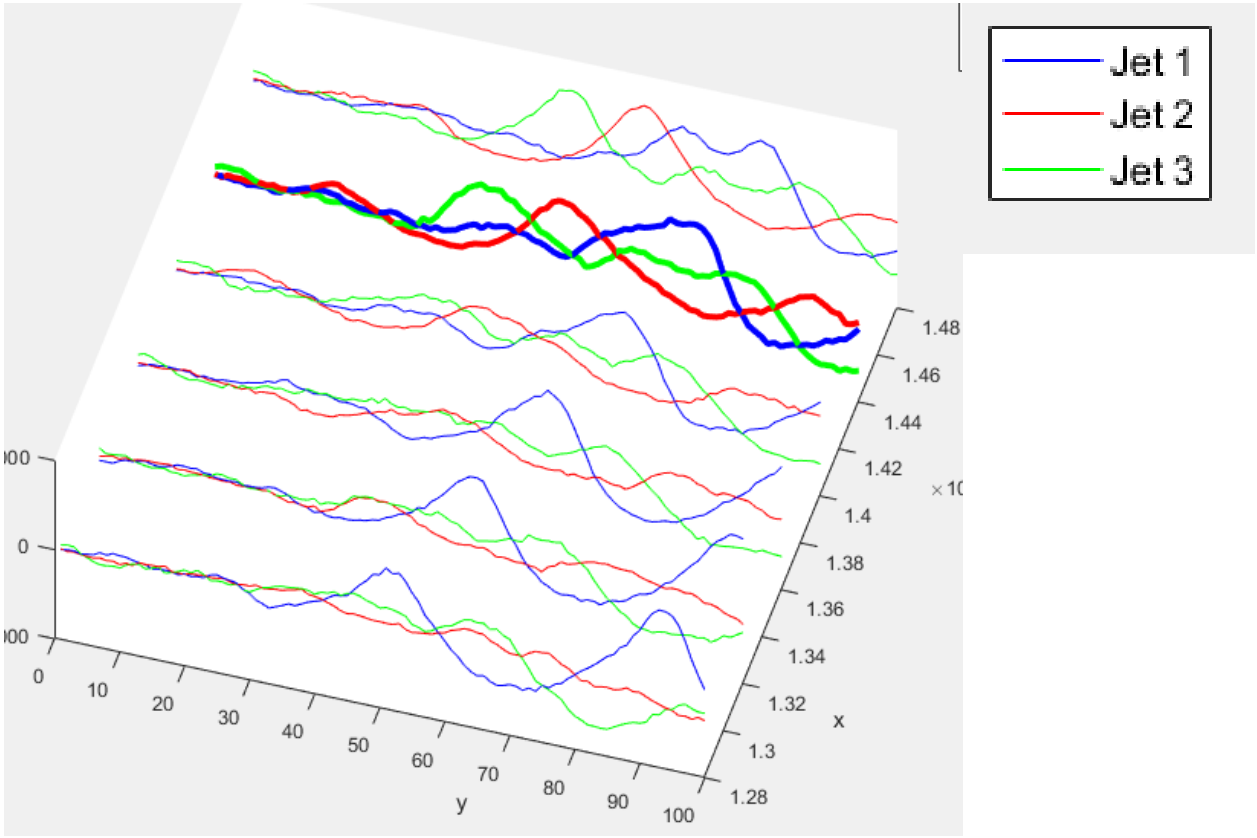

As one wave structure travels downstream, the other two jets response to the downstream flow disturbance.

Pressure Node Forced (2 Psi)

Shadowgraph

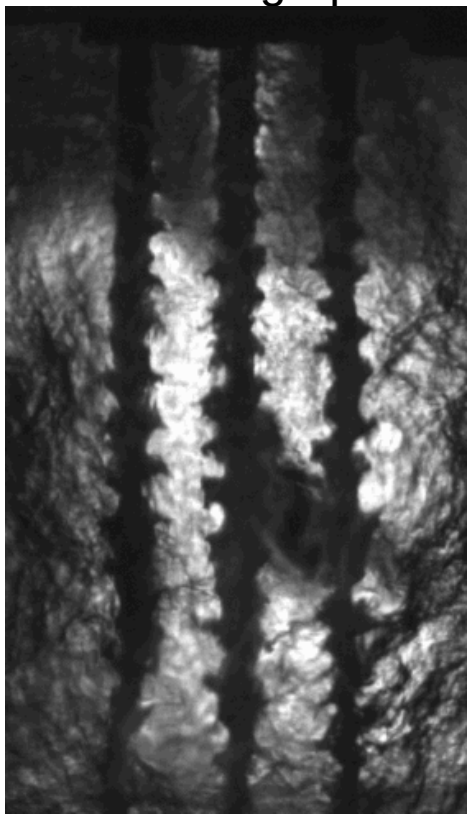

OH*

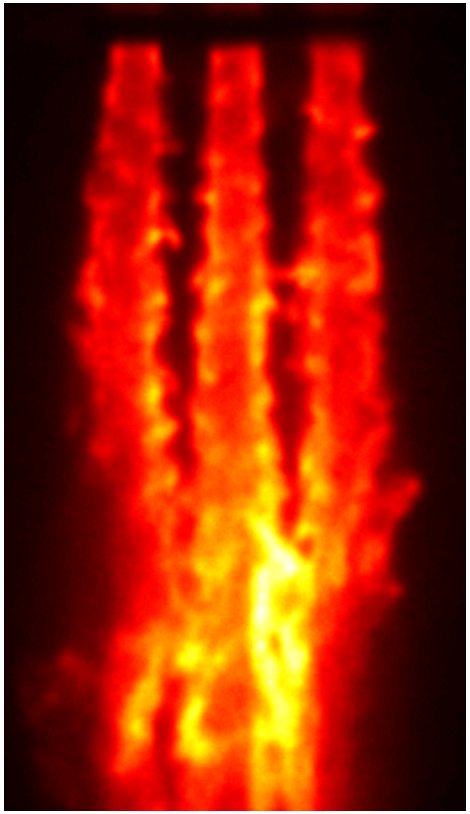

FUSED

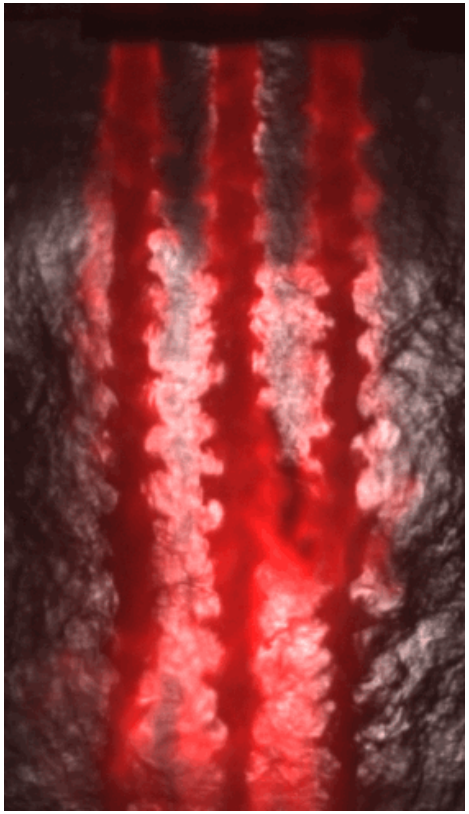

- Pressure node forcing does not appear to deflect the LOX jet, but it developed lobes.
- The flame develops a flapping motion.

Pressure Node Forced (2 Psi)

FUSED | Shadowgraph | OH*

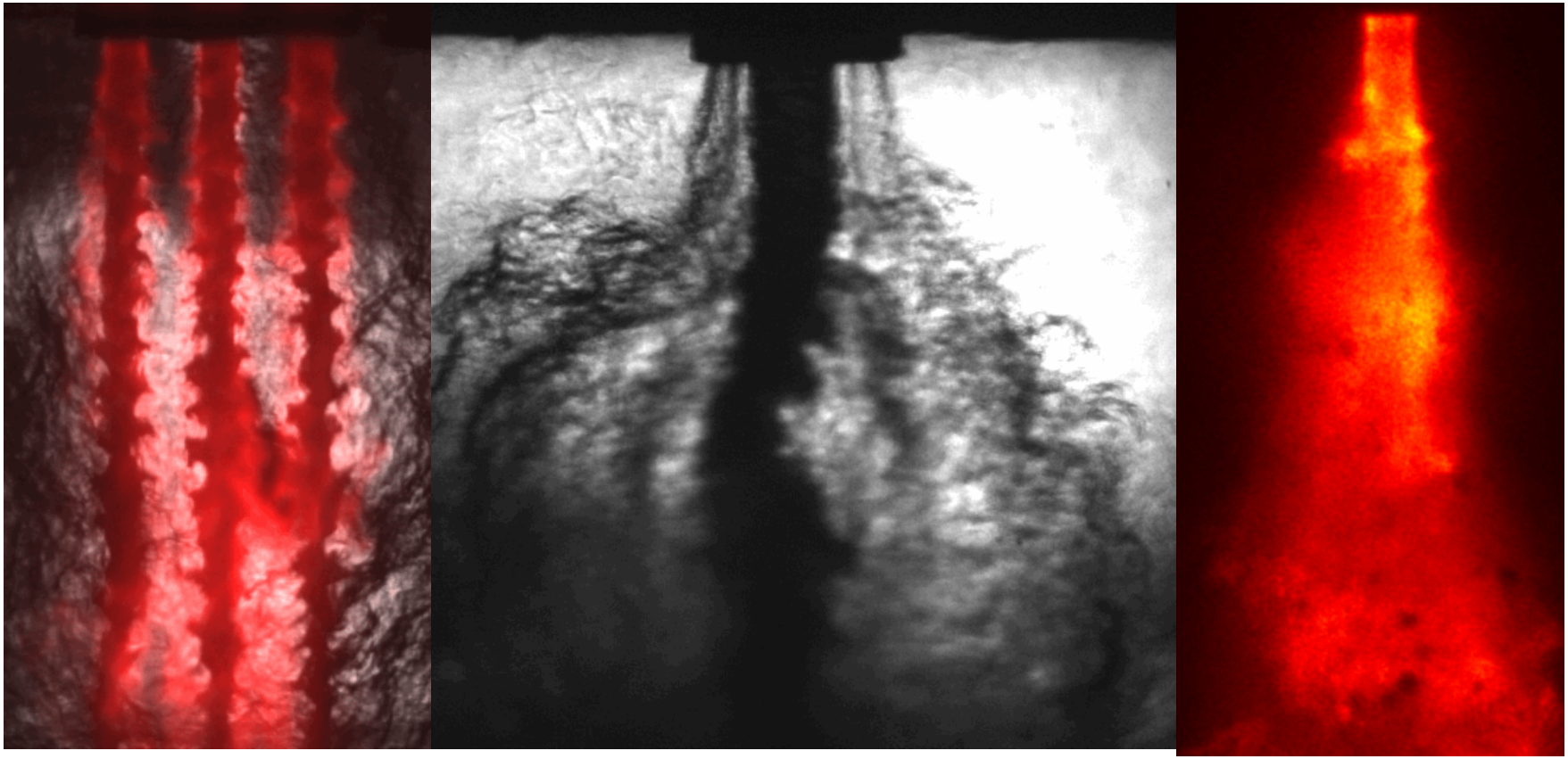

- Zooming on the single element, the hydrogen jet is displaced towards the LOX jet.
- (Images are not one to one)

Pressure Node Forced (2 Psi)

FUSED | Shadowgraph | OH*

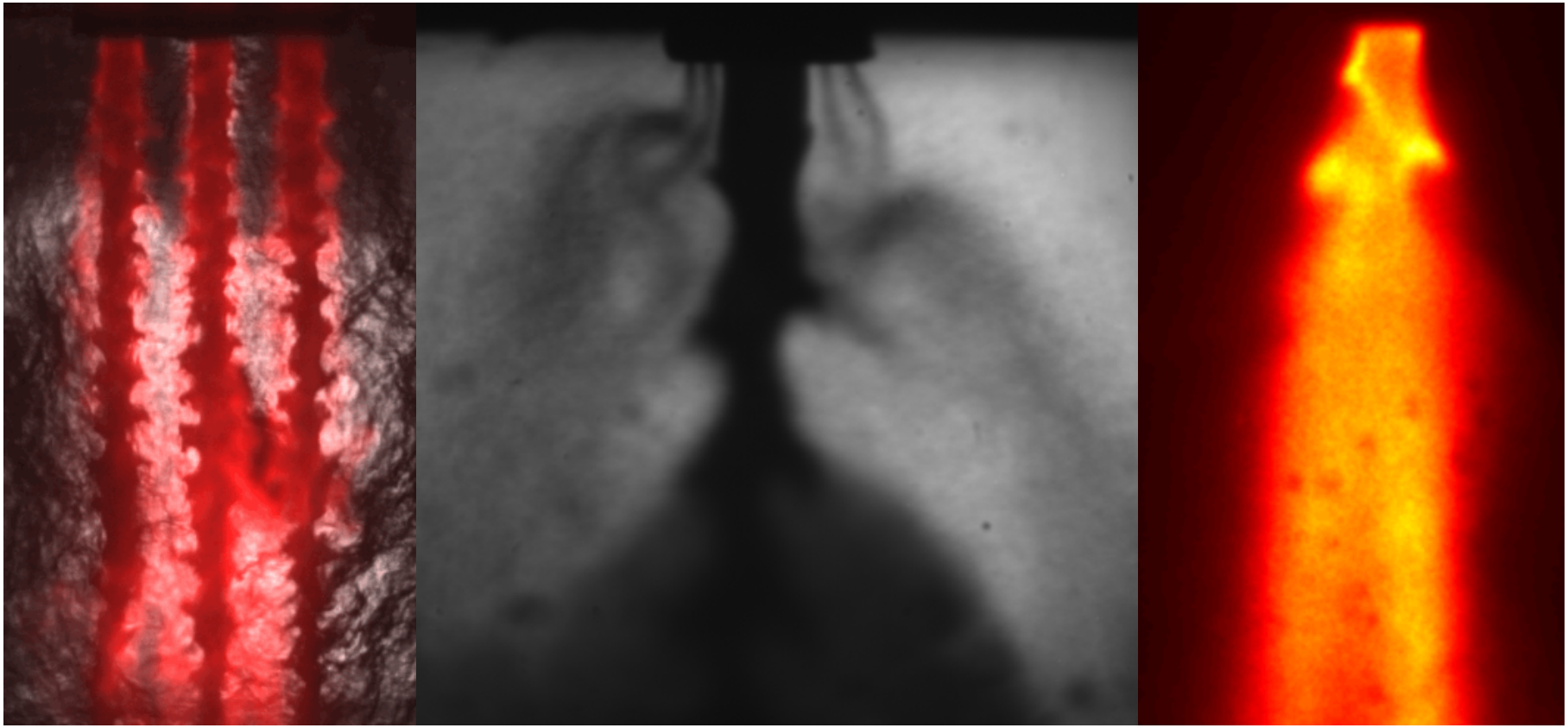

- Phased average of the single element flow. Zooming on the single element, the hydrogen jet is displaced towards the LOX jet.
- (Images are not one to one)

Pressure Node Forced (2 Psi)

- The strong DMD amplitude detects the acoustic forcing and high harmonics.
- The flow has strongly coupled with the acoustic forcing.
- The transverse acoustic velocity perturbations results in slants bands for the OH*. This is a result of the in-plane flapping motion shown in the raw images.
- Further downstream, the waves on the liquid oxygen jet are offset from each other.

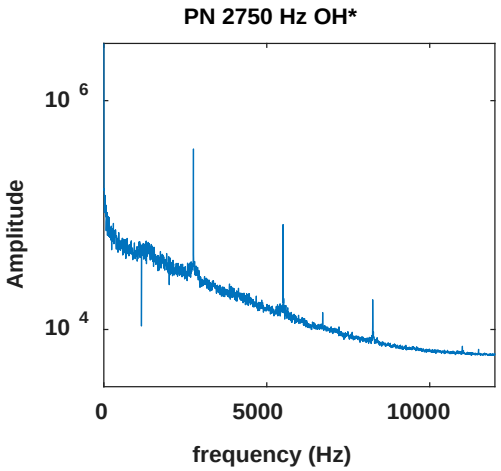

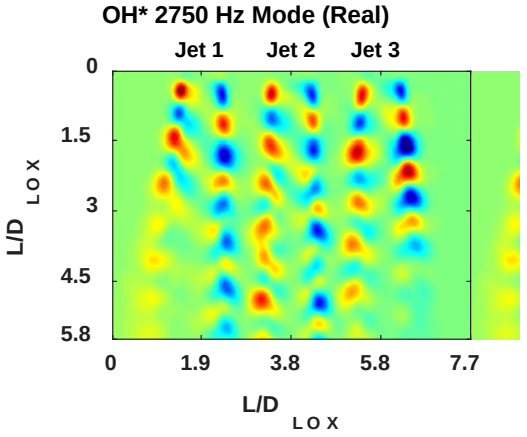

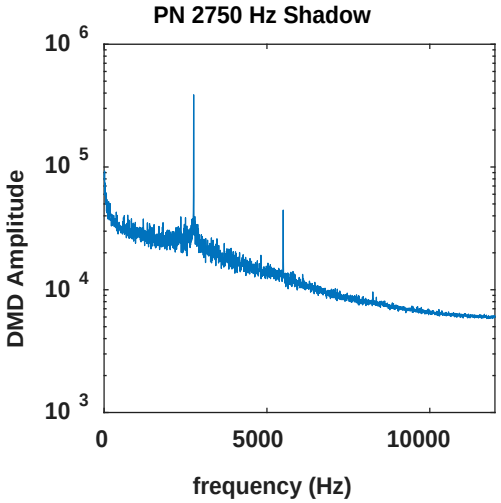

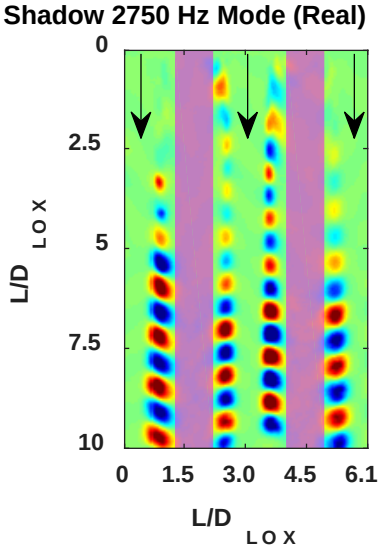

Conclusion

- Flame is attached at the nozzle exit.
- From the spectral analysis of the OH* fluctuations, the 3 injectors do indeed interact and share a similar frequency. The center injector is out of phase with its neighbors.
- The DMD analysis of the unforced condition showed that physical features of the flow are offset or out of phase.
- OH* tracking points to when one injector creates a flow disturbance the other two response.
- The DMD analysis detected strongly coupled flow with the acoustic forcing.
- The DMD spatial modes demonstrates the OH* emission has a flapping motion and the waves on the liquid oxygen surface are offset from each other.

Future Work

- Increase window survivability rate.
- Perform a sensitivity study with acoustic forcing.
  - At what pressure amplitudes does the multi-element injector couple with the acoustic field.
  - Perform this study for a different range of frequencies, phases, and operating conditions.
- Perform Mie scattering of the hydrogen jet to track the vortex structures shed close to the nozzle.

Questions?